NASA SP-315

APOLLO 16

Preliminary Science Report

PREPARED BY

NASA MANNED SPACECRAFT CENTER

Scientific and Technical Information Office 1972

NATIONAL AERONAUTICS AND SPACE ADMINISTRATION

Washington, D.C.

8. Soil Mechanics

James K. Mitchell,[a†] W. David Carrier, III,[b] William N. Houston,[a]
Ronald F. Scott,[c] Leslie G. Bromwell,[d] H. Turan Durgunoglu,[a]
H. John Hovland,[a] Donald D. Treadwell,[a] and Nicholas C. Costes[e]

INTRODUCTION

The purpose of the soil mechanics experiment is to determine the physical characteristics and mechanical properties of the lunar soil to depths of several decimeters and their variations in lateral directions, on slopes, and between different regions of the Moon. Measurements using a self-recording penetrometer (SRP), in conjunction with observational data and information on soil characteristics obtained from returned samples, have enabled determination of parameters for density profiles, porosity profiles, and strength parameters.

An understanding of lunar-soil properties is important to lunar studies such as (1) formation and compaction of surface layers, (2) characterization of deposits of different composition, (3) slope stability and downslope movement of soil and rock fragments, (4) prediction of seismic velocities, (5) estimation of thermal properties for use in heat-flow studies, (6) characterization of dielectric properties for use in radar-backscatter and electrical-property studies, (7) gas diffusion through the lunar surface, (8) definition of appropriate conditions for later terrestrial-simulation studies, and (9) various types of soil-property-dependent engineering analyses.

The Apollo 16 mission has made it possible to study a lunar highlands area and to compare the properties of the soil on slopes (as exemplified by the soil blanketing the Descartes material on Stone Mountain to the south of the lunar module (LM) landing point) with properties of the soil covering the Cayley Plains in the vicinity of the LM.

Although many of the analyses and results presented in this report are preliminary and more detailed analyses and simulations are planned, it appears that objectives of the experiment have been achieved, as discussed in the following subsections.

SUMMARY OF PREVIOUS RESULTS

The mechanical properties of lunar soil as deduced to date have been summarized by Mitchell et al. (ref. 8-1) who note that the soil behavior is similar to that of terrestrial soils of comparable gradation, even though the two soil types are compositionally dissimilar. Particle-size distribution, bulk density, and particle shape appear to control physical behavior.

A variety of data sources indicates that the soil porosity, density, and strength vary locally and with depth. Densities may be in the range of 1.0 to 2.0 g/cm^3, and values greater than 1.5 g/cm^3 are probable at depths of 10 to 20 cm. Despite these local variations, however, Houston et al. (ref. 8-2) have found that the mean porosity at each of the previous Apollo landing sites was the same (43.3 percent) for the upper few centimeters of soil. The soil on crater rims and on crater and rille slopes was found to have a somewhat higher porosity (an average value of 46 to 47 percent). Apollo 15 results (ref. 8-3) also suggest somewhat lower densities for soil on slopes.

For a given lunar soil, porosity appears to be the most important single variable controlling the strength parameters, with most probable values lying in the range of 0.1 to 1.0 kN/m^2 for cohesion and 30° to 50° for friction angle; the higher values are associated with lower porosities. Data from Lunokhod-1 (ref. 8-4) indicate that strength (and therefore density) increases with depth.

[a]University of California at Berkeley.
[b]NASA Manned Spacecraft Center.
[c]California Institute of Technology.
[d]Massachusetts Institute of Technology.
[e]NASA Marshall Space Flight Center.
[†]Principal Investigator.

METHODS AND THEORY

Data Sources

Soil mechanics data were derived from (1) crew commentary and debriefings, (2) television, (3) lunar-surface photography, (4) performance data and observations of interactions between soil and the lunar roving vehicle (Rover), (5) drive-tube and deep drill samples, (6) sample characteristics as determined by the Lunar Sample Preliminary Examination Team (LSPET), and (7) measurements using the SRP.

The core drive tubes used for Apollo 16 are the same type as those used for Apollo 15. The individual thin-walled tubes are 37.5 cm long and have an inside diameter of 4.13 cm and an outside diameter of 4.38 cm. Tubes can be used singly or in combination (double-core tubes).

The SRP (fig. 8-1), the main quantitative data source for the soil mechanics experiment, was used to obtain data on soil-penetration resistance as a function of depth below ground surface. Maximum possible penetration depth of the SRP is 76 cm, and the maximum recordable penetration force is 215 N. The record of each penetration is inscribed on a recording drum contained in the upper housing assembly. The lunar-surface reference plane rests on the lunar surface during a measurement and serves as a datum for measurement of penetration depth. A 2.54- by 12.7-cm bearing plate and two penetrating cones, each of 30° apex angle and base areas of 1.29 and 3.22 cm^2, were available for attachment to the penetration shaft.

Quantitative Determination of Soil Properties

The results of simulation studies (refs. 8-2 and 8-5 to 8-8) and soil mechanics theories (ref. 8-9) are used as a basis for the deduction of quantitative values of soil properties.

Soil-strength parameters are deduced from the results of the penetration tests in the following way, as shown by Durgunoglu (ref. 8-10). From the results of model tests, it has been found that a failure surface as shown in figure 8-2 represents closely the actual

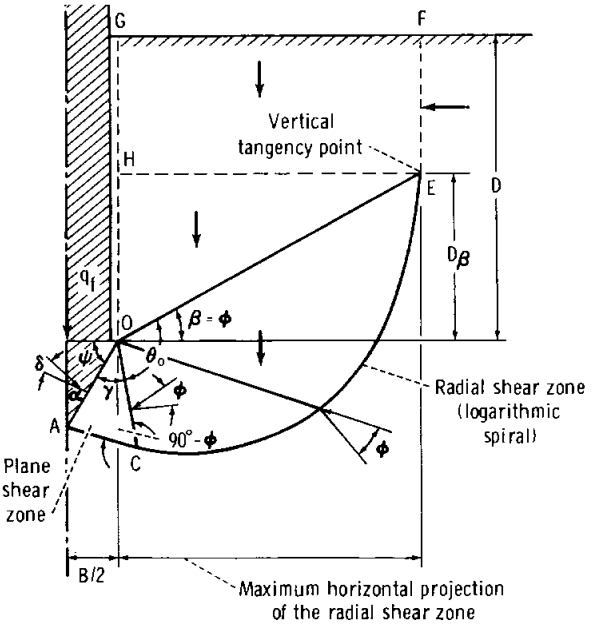

FIGURE 8-2.–Failure mechanism associated with wedge penetration. (Symbols used in this figure are defined in the appendix.)

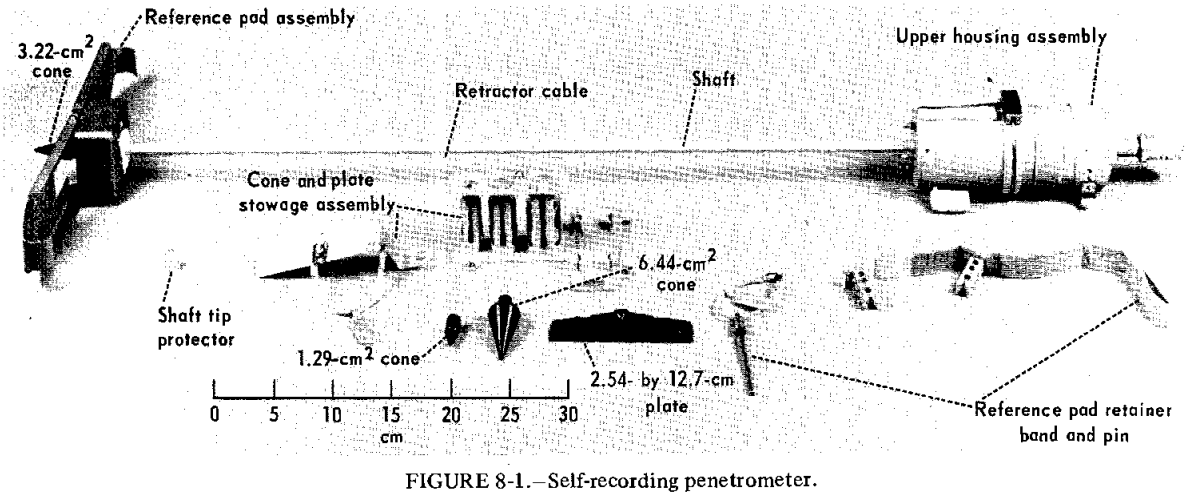

FIGURE 8-1.–Self-recording penetrometer.

failure surface associated with wedge penetration into relatively dense, fine, sandy soils. Equilibrium analysis of the failure zone shown in figure 8-2 leads to

$$q_f = cN_c\xi_c + B\gamma_s N_{\gamma q}\xi_{\gamma q} \qquad (8\text{-}1)$$

where

q_f = ultimate unit tip resistance (force divided by base area)
c = unit cohesion
B = penetrometer base width or diameter
γ_s = unit weight of soil = ρg
ρ = soil density
g = acceleration due to gravity
N_c, $N_{\gamma q}$ = bearing capacity factors = f(D/B, ϕ, α, δ/ϕ)
ξ_c,$\xi_{\gamma q}$ = shape factors
D = depth of penetrometer (wedge) base below ground surface
α = half the wedge apex angle
δ = soil-to-penetrometer friction angle
ϕ = soil friction angle

The value of δ/ϕ has been taken as 0.5, based on the results of friction measurements between a ground-basalt lunar-soil simulant and hard anodized aluminum similar to that used for the SRP cones. Equations for evaluation of the factors N_c and $N_{\gamma q}$ are given in the appendix, and charts for N_c and $N_{\gamma q}$ as a function of ϕ for a range of values of D/B, α, and δ/ϕ are in reference 8-10.

The ultimate penetration resistance of cones is best estimated by using the bearing capacity factors for wedges modified by shape factors. The appropriate equations are

$$\xi_c = 1 + \left(0.2 + \tan^6\phi\right)\frac{B}{L} \text{ for } \phi \geq 25° \qquad (8\text{-}2)$$

$$\xi_{\gamma q} = \left(1.0 - 0.4\,\frac{B}{L}\right) + \frac{1.5}{\frac{B}{D} + \frac{1.5}{\left(0.6 + \tan^6\phi\right)\frac{B}{L}}} \qquad (8\text{-}3)$$

where L is the length of the loaded area and B/L = 1.0 for the SRP cones and 0.20 for the SRP bearing plate.

Infinite combinations of c and ϕ could satisfy equation (8-1) for a given penetration resistance and depth. If penetration resistance values are available for two sizes of cone penetrating the same soil conditions or if the soil deposit is homogeneous and the penetration resistance is known at two depths, then specific values of c and ϕ may be determined by simultaneous solution of two equations of the form of equation (8-1), one for each combination of q_f and D/B values.

RESULTS

General Soil Characteristics at the Descartes Site

Soil cover is present at all points visited in the Descartes landing area. The surface is similar in color (gray and gray-brown) to that at other Apollo sites, although white soil layers were encountered at shallow depths in some areas (e.g., near Flag and Spook Craters and on Stone Mountain). The full lateral extent of this lighter colored (and coarser) material is unknown. Surface textures range from smooth areas almost free of rock fragments through patterned ground to areas heavily populated by larger rocks and fragments.

Substantial variability in soil properties exists from point to point, both regionally and locally. Various quantitative aspects of this variability are discussed in detail subsequently. Figures 8-3, 8-4, and 8-5 provide qualitative indications of local variations in soil properties, as evidenced by differing depths of footprints. The deeper the footprint, the less dense, the weaker, and the more compressible is the soil near the surface. In general, the soil on Stone Mountain (fig. 8-3) was found to be softer and less dense than that in the area including the LM and the Apollo lunar-surface experiments package (ALSEP) (fig. 8-4), which in turn was less strong and less dense than that at station 13, south of the rim of North Ray Crater (fig. 8-5), even though the local variations at any station were significant.

Soil behavior during landing, walking, driving, and sampling was comparable to that observed during the earlier missions. Dust was readily kicked up under foot and by the Rover and tended to adhere to surfaces with which it came in contact. Visibility degradation by blowing dust during the LM descent and landing was less than that of previous missions, probably because of (1) a faster rate of descent and, therefore, a reduced time for erosion and (2) a higher Sun angle, rather than because of any significant difference in soil characteristics.

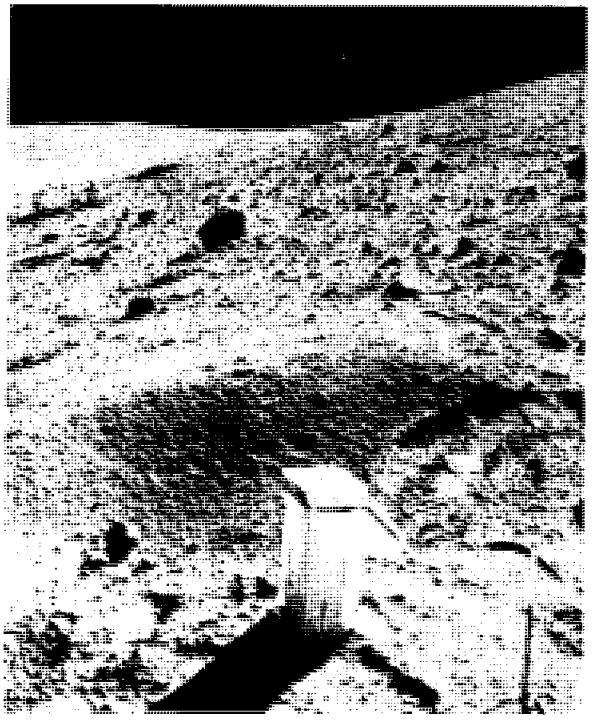

FIGURE 8-3.–Variable soil conditions at station 4 on Stone Mountain (AS16-107-17474).

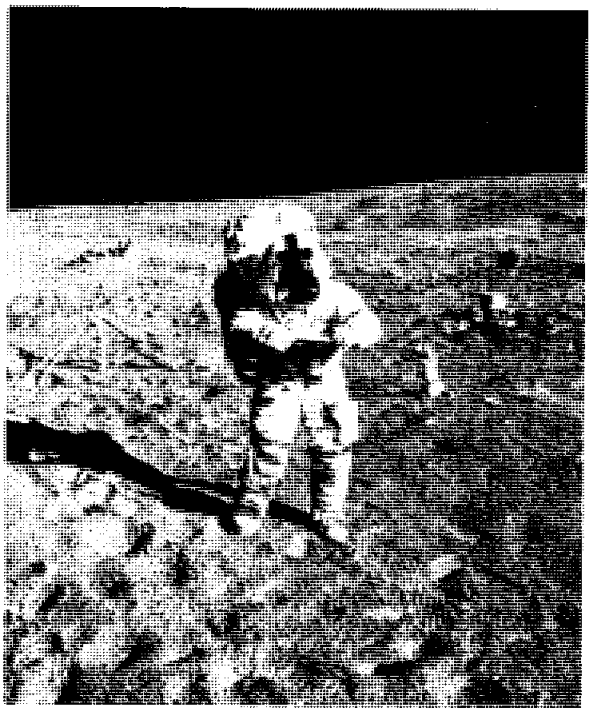

FIGURE 8-4.–Variable soil conditions in the ALSEP area (AS16-114-18387).

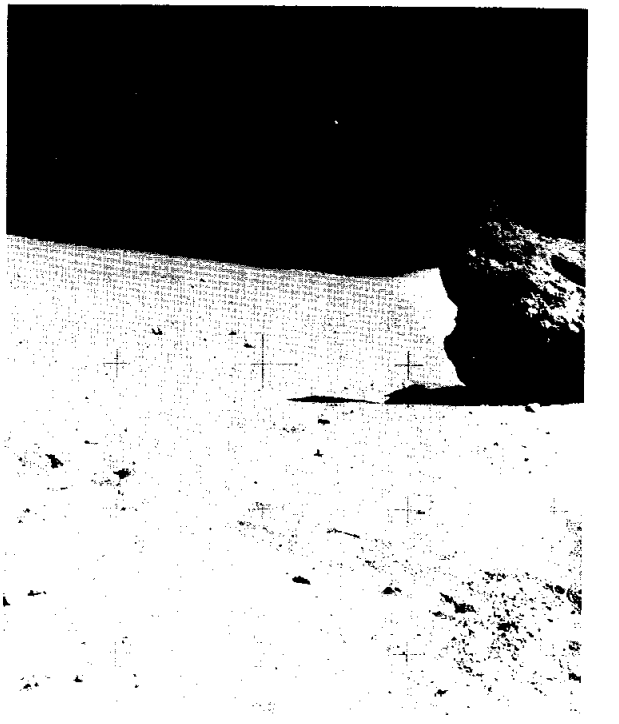

FIGURE 8-5.–Variable soil conditions at station 13 south of North Ray Crater (AS16-106-17392).

Grain-size data have been obtained by the LSPET for samples from several locations. Some of these data curves are shown in figure 8-6 and are compared with a composite distribution for Apollo 11, 12, 14, and 15 samples. The two samples from station 11 (North Ray Crater) are distinctly coarser than the samples from the other stations and coarser than the composite distribution. This may be the result of a significantly lower exposure age, similar to the Apollo 12 double-core-tube coarse-soil layer and the Apollo 14 Cone Crater and trench samples.

The other Apollo 16 samples that have been analyzed to date tend to fall toward the coarser edge of the composite distribution, primarily due to the larger proportion of 10-mm particles which, in many cases, weighed more than the 4-mm and 2-mm fractions. This is probably attributable to an abundance of South Ray Crater rocks that have not yet been worked into the soil matrix. Also shown in figure 8-6 are limited data from Luna 16 (ref. 8-11), which fall within the composite distribution value range.

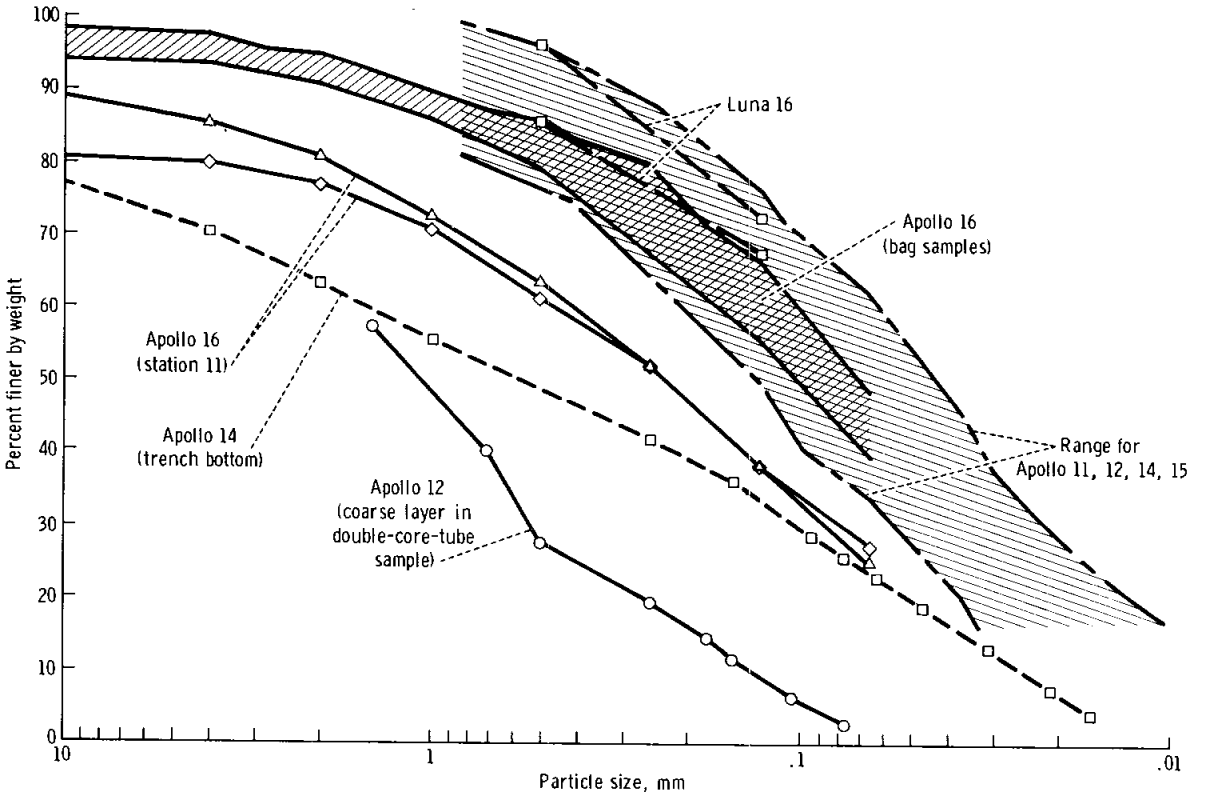

FIGURE 8-6.–Grain-size-distribution curves for several Apollo 16 samples compared with composite distribution for samples from Apollo 11, 12, 14, and 15 missions and from two Luna 16 samples.

Core Samples

Drive tubes.–More than 6 kg of drive-tube samples were obtained in the form of double-core-tube samples from stations 4, 8, 10, and 10′ (fig. 6-4, section 6) and a single-core-tube sample from station 9. The X-radiographs of the as yet unopened tubes indicate that the lunar stratigraphy and soil fabric have been well preserved.

Data on the drive-tube samples are summarized in table 8-I. The core-recovery percentages are comparable to those of the Apollo 15 samples, for which the same type of core tube was used. The double-core-tube data in table 8-I indicate, in all cases, that the soil density in the lower tube is greater than that in the upper tube; that is, density increases with depth. The range of densities (1.40 to 1.80 g/cm^3) is slightly less than that found for the Apollo 15 samples (1.36 to 1.91 g/cm^3).

Drill stems.–The deep core was drilled to a total depth of 2.24 ± 0.03 m in the ALSEP area, located as shown in figure 6-4, section 6. Resistance to drill advance was not great; in fact, the lunar module pilot (LMP) deliberately held up on the drill head to slow the rate of drilling. The first section of core was drilled at a rate of approximately 150 cm/min, whereas subsequent drilling was at a rate of approximately 60 to 75 cm/min.

After the drill stem was withdrawn, the "rammer-jammer" from the heat-flow experiment was dropped into the open hole. It dropped to a depth of about 2.18 m, indicating that the hole had remained open to within approximately 6 cm of the bottom. It is not known whether the hole closed below this depth because of soil failure resulting from insufficient strength in the bottom of the hole, because some sample fell out of the drill stem during withdrawal, or because of side-wall raveling during withdrawal.

TABLE 8-I.–Preliminary Data on Apollo 16 Drive-Tube Samples

Station	Serial no.	Sample no.	Sample weight, g	Sample length, cm (a)	Bulk density, g/cm^3	Tube depth (pushed), cm	Total depth (pushed and driven), cm	No. of hammer blows	Core recovery, percent
4	[b]2043	64002	584.1	31.7	[c]1.38 to 1.40	32.6 ± 0.5	[d]65 ± 6	≫3	103 ± 10
	2038	64001	752.3	[e]33.9	1.66				
8	2029	68002	583.5	27.4	1.59	17.8 ± 0.5	68.6 ± 0.5	~56	91
	2036	68001	840.7	34.9	1.80				
9	2034	69001	558.4	–	–	20.6 ± 0.5	[d]27.5 ± 2	8	–
10	[b]2045	60010	635.3	32.3	1.47	17.9 ± 0.5	[d]71 ± 2	~53	95 ± 3
	2054	60009	759.8	[e]33.1	1.72				
10	2027	60014	570.3	[c]28.8 to 28.4	1.48	28 ± 2	70.5 ± 1	27	90 ± 1
	2032	60013	757.2	[e]34.7	1.63				

[a]Measured from X-radiographs taken by the LSPET.

[b]Crewmen neglected to insert keeper.

[c]Corrected for void.

[d]Measured from kinescopes.

[e]The nominal length of the sample in a lower core tube is 34.9 cm; for those tubes in which the actual sample length is less, either some sample fell out or the keeper compressed the top of the sample. The former is considered to be the more likely explanation, and the densities have been calculated accordingly. The internal diameter of the core tubes is 4.13 cm.

Data for the samples contained in the six drill-stem sections are given in table 8-II. From these data and X-radiographs of the stems, it is known that the top section is half full; the second section is nearly full with a 5-cm-long void at the bottom; the third section is nearly empty, and what little sample it does contain is distributed along its length. The fourth, fifth, sixth, and bit sections are full.

Several hypotheses have been proposed to account for the sample distributions in the different sections. The most plausible explanation at the present time is that the initial core recovery was only about 88 percent because of the low density and high penetration rate near the surface, leaving a void of approximately 1-1/2 sections in the top three sections when the drill stem was separated into two three-section lengths for Earth return. During lunar lift-off, zero-g travel, entry into the Earth atmosphere, splashdown, and transport to and handling in the Lunar Receiving Laboratory, the sample migrated up the sections, finally becoming distributed in various states of compaction over a length of 2-1/2 sections.

TABLE 8-II.–Preliminary Data on Apollo 16 Drill-Stem Sections

Drill-stem serial no.	Sample no.	Sample mass, g	Sample length, cm	Bulk density, g/cm^3	Drill-stem depth, cm
014	60007	105.7	22.2	1.46	224 ± 3
012	60006	165.6	35.5 ± 0.5	1.43 ± 0.02	
024	60005	76.1	–	–	
015	60004	202.7	39.9	1.56	
019	60003	215.5	39.9	1.66	
018	60002	211.9	42.5	1.75	
180 (bit)	60001	30.1			

Penetrometer Test Results

Eleven tests were made using the SRP during the second extravehicular activity period. Four cone-penetration tests were made at station 4 on Stone Mountain; five cone-penetration tests and two plate-load tests were made in the station 10-ALSEP area. The nature of each of these tests is summarized in table 8-III. A planimetric sketch map of station 4 showing the penetrometer test locations is presented in figure 8-7. Similar information for the station 10 area is given in figure 8-8.

Curves representing penetration resistance as a function of depth are plotted in figure 8-9 for cone-penetration tests at station 4, in figure 8-10 for cone-penetration tests at station 10, and in figure 8-11 for plate-load tests at station 10. In each case, the raw data as taken directly from the SRP recording drum are presented. A visual record of all tests except the first cone-penetration test at station 4 and the first plate-load test at station 10 was obtained by the lunar-surface television camera. From a detailed study of the kinescopes, it is clear that the spikes shown on several of the penetration curves, which reflect sudden unloading and reloading, were a direct consequence of the test procedure and not of the soil conditions. These spikes can be ignored in the interpretation of test results. However, where the penetration curves show a simultaneous reduction in stress and an increase in penetration, as in figures 8-9(d), 8-10(c), and 8-10(d), it is a reflection of softer soil layers, as discussed later in more detail.

As shown in figures 8-9, 8-10, and 8-11, an intercept for zero stress on the penetration axis is present in each test. This intercept ranges between 1.9 and 9.0 cm. Careful study of the kinescopes and the test procedures used on the lunar surface indicates that these intercepts most likely resulted from the lunar-reference plane (fig. 8-1) riding up on the penetrometer shaft after initial indexing and positioning. The LMP repositioned the reference plane after each test and before moving to the next test location. As he moved to the next test area, the penetrometer tip was pointed slightly upward. Coupled with movement of the LMP and the sensitive balance between the reference plane and retractor cable, some detectable movement of the reference plane up the shaft occurred. In addition, placing the SRP onto the lunar surface while holding it by the housing could have led to some penetration (because of inertial effects) without recording the accompanying force. Thus, the penetration curves do not reflect soil conditions above the intercept point, but they are correct below it.

TABLE 8-III.–Summary of Penetration Tests Determined From SRP Data

Station	*Test no.*	*SRP index no.*	*Penetrometer tip*	*Location*	*Maximum penetration depth, cm*	*Maximum force to reach maximum depth, N*
4	1	5	3.22-cm^2 cone	Uphill, south of Rover	21.3	215
4	2	6	1.29-cm^2 cone	On bench, south of Rover (near edge of subdued crater)	74	53.5
4	3	7	1.29-cm^2 cone	On bench, southwest of Rover (near edge of subdued crater)	46	215
4	4	8	1.29-cm^2 cone	Downhill, north of Rover (next to double-core tube)	73	199
10	1	10	3.22-cm^2 cone	Near Rover	22	>215
10	2	11	1.29-cm^2 cone	Near Rover (next to double-core tube)	50.5	>215
10	3	12	1.29-cm^2 cone	Southwest of Rover on line to deep drill core	42	>215
10	4	13	1.29-cm^2 cone		62.5	199
10	5	14	1.29-cm^2 cone		70	(a)
10	6	15	2.54- by 12.7-cm plate	Near Rover (next to double-core tube)	9.7	>215
10	7	16	2.54- by 12.7-cm plate	Near Rover	6.3	>215

[a]No data recorded on SRP drum.

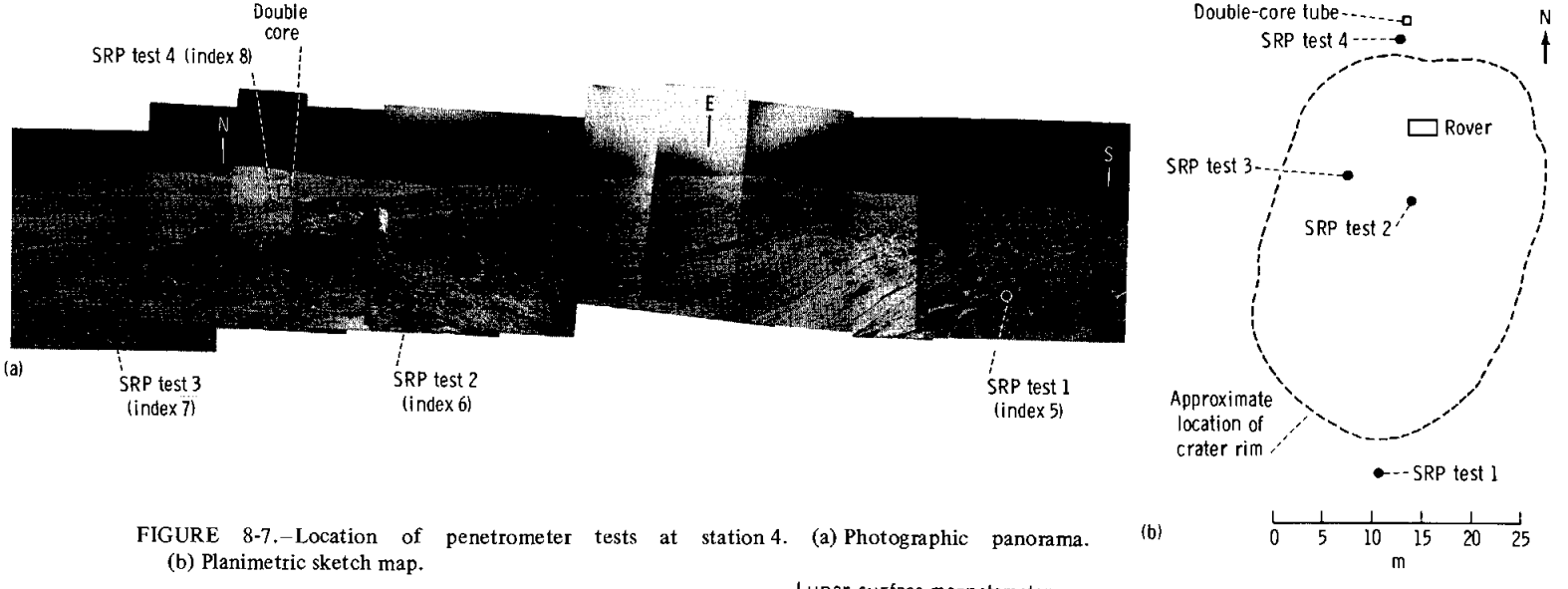

FIGURE 8-7.–Location of penetrometer tests at station 4. (a) Photographic panorama. (b) Planimetric sketch map.

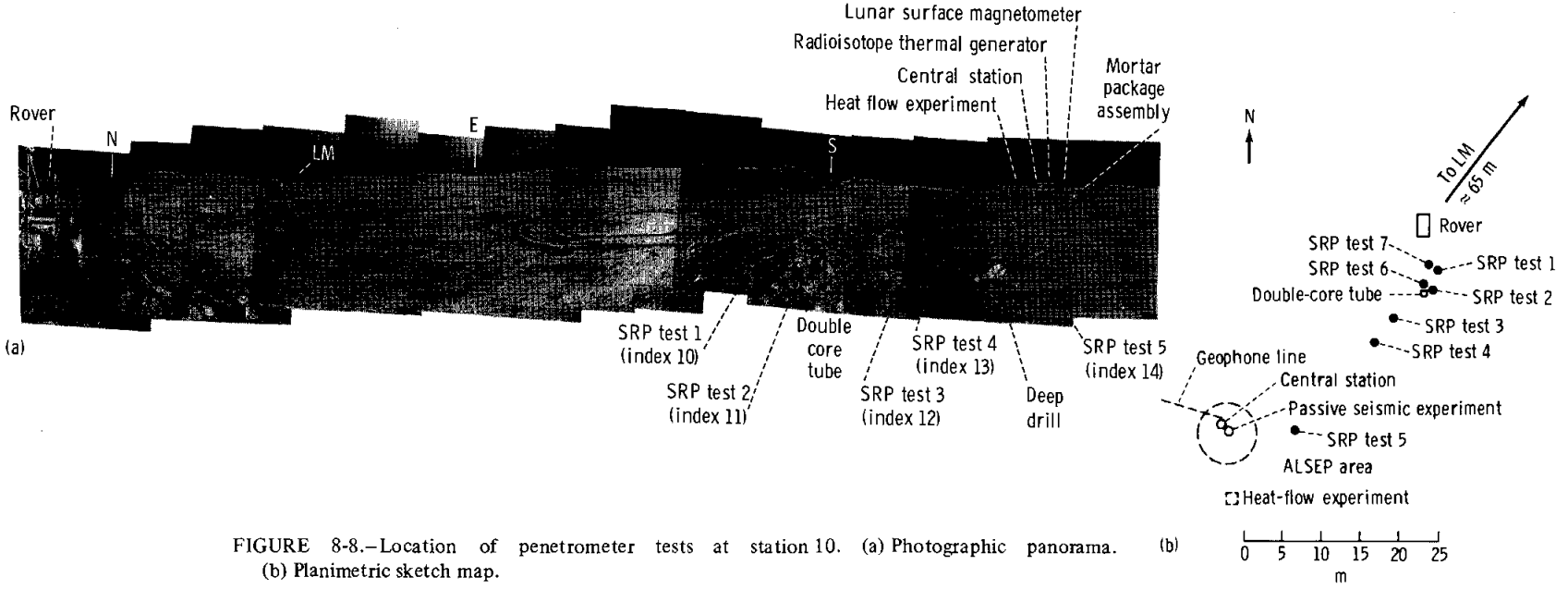

FIGURE 8-8.–Location of penetrometer tests at station 10. (a) Photographic panorama. (b) Planimetric sketch map.

As indicated in table 8-III, data on force as a function of penetration for test 5 at station 10 (index 14) did not record. Analysis of the kinescopes and the performance characteristics of the penetrometer suggests that this probably was because the LMP had placed his left hand around the upper housing assembly in such a manner that the indexing lever was depressed, thus locking the recording drum and preventing inscription of the test data.

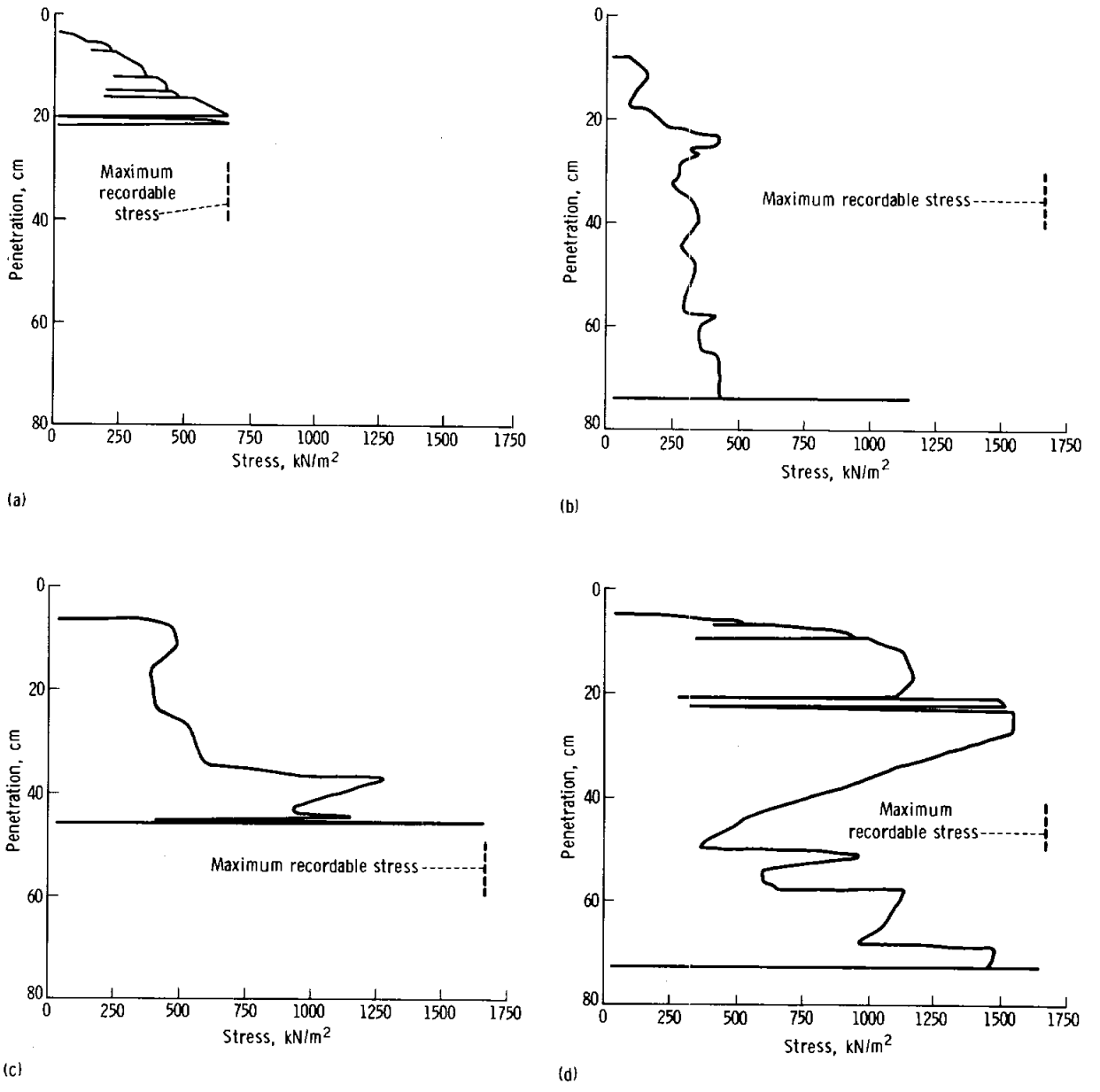

FIGURE 8-9.–Cone-penetrometer-test results for station 4. (a) Test 1, 3.22-cm^2 cone, index 5. (b) Test 2, 1.29-cm^2 cone, index 6. (c) Test 3, 1.29-cm^2 cone, index 7. (d) Test 4, 1.29-cm^2 cone, index 8.

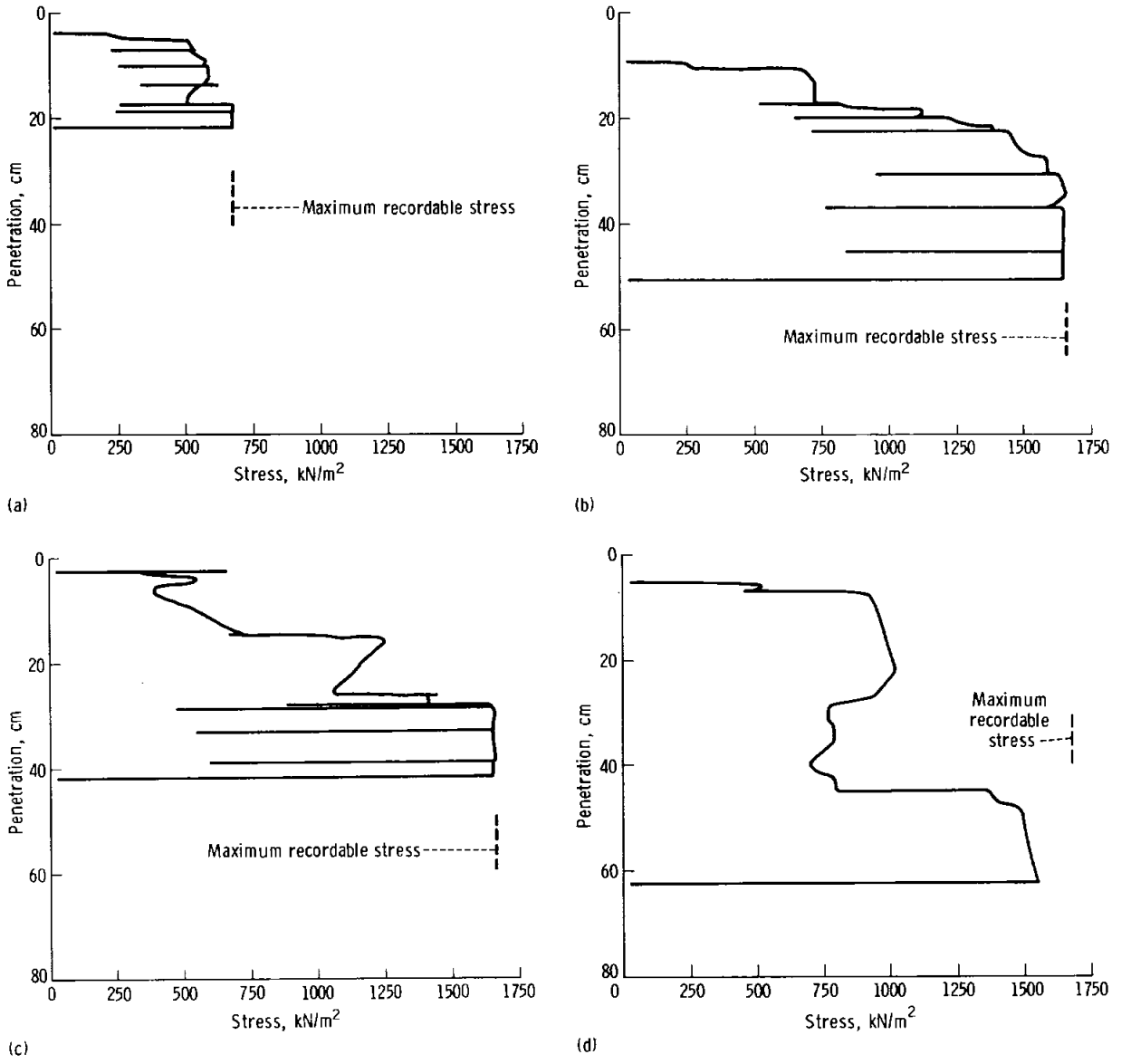

FIGURE 8-10.—Cone-penetrometer-test results for station 10. (a) Test 1, 3.22-cm^2 cone, index 10. (b) Test 2, 1.29-cm^2 cone, index 11. (c) Test 3, 1.29-cm^2 cone, index 12. (d) Test 4, 1.29-cm^2 cone, index 13.

DISCUSSION

Stratigraphy and Variability

The penetration curves in figures 8-9, 8-10, and 8-11 may be used to construct details of the lunar soil to depths of a few decimeters beneath the surface. The rather marked differences among the shapes of the curves are a direct qualitative indication that soil conditions are locally variable. Some characteristics at each test location may be noted.

Station 4 (Stone Mountain).—Penetration test 1 (index 5), made uphill to the south of the Rover, indicates a relatively homogeneous soil to a depth of approximately 20 cm. A smoothed curve fit to the

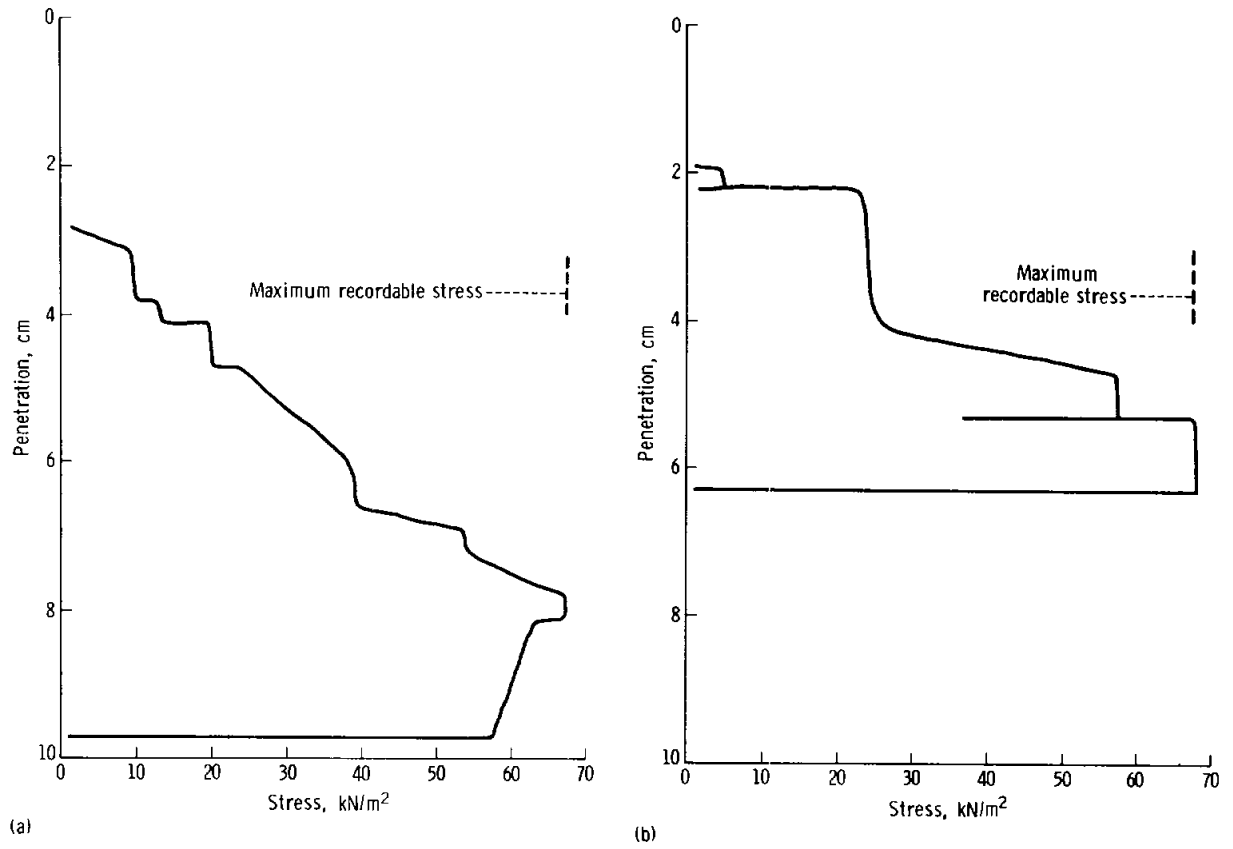

FIGURE 8-11.–Plate-load-test results for station 10. (a) Test 6, 2.54- by 12.7-cm plate, index 15. (b) Test 7, 2.54- by 12.7-cm plate, index 16.

data in figure 8-9(a) is characteristic of that for a dominantly frictional soil with low cohesion.

Penetration test 2, index 6 (fig. 8-9(b)), indicates a much softer soil in the area a few meters south of the Rover. From the photographs (fig. 8-7(a)), the test appears to have been made in an area near the edge of the subdued crater in which the Rover was parked. A layer of higher resistance is indicated at a depth of approximately 24 cm.

From figure 8-9(c), it is evident that a highly resistant layer was encountered at a depth of 45 cm during test 3 (index 7). The soil was stronger, in general, than that observed for test 2. The location for test 3 was southwest of the Rover, also near the rim of the subdued crater.

Test 4 (index 8) was made downhill to the north of the Rover. The penetration curve (fig. 8-9(d)) indicates a very dense and resistant layer extending to a depth of approximately 27 cm. Softer soil was located below this layer to a depth of approximately 50 cm, where firm material was again encountered. To test this interpretation, a simulation test was done on a model soil composed of a soft, weak layer sandwiched between two firm, strong layers. The curve for penetration resistance as a function of depth for this condition is shown in figure 8-12. It is comparable to the curve in figure 8-9(d).

A double-core drive-tube sample was taken at a point near (1 m) the location of penetration test 4. The X-radiograph of the core sample reveals layers that correlate well with the penetration curve in figure 8-9(d). The interpretations made of the soil conditions in the core sample by J. S. Nagle of the LSPET are shown in figure 8-13. Nagle suggests that the coarse-grained layer with abundant rock fragments decreasing with depth is South Ray Crater material and that the Descartes deposit underlies the South Ray layer. This layer is clearly delineated in

figure 8-13 and implies that the Descartes material is at least 45 cm below the surface at the site of test 3, index 7 (fig. 8-9(c)); that the South Ray material is very thin and the Descartes deposit begins at 30 cm at the test 2 site, index 6 (fig. 8-9(b)); and that the Descartes material is at least 21 cm below the surface at the test 1 site, index 5 (fig. 8-9(a)).

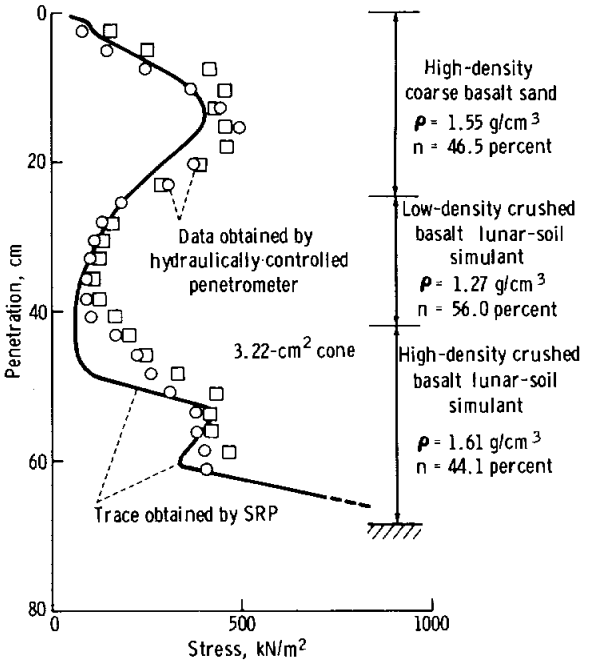

FIGURE 8-12.–Penetration resistance as a function of depth relationship for a soft soil layer sandwiched between two firm layers.

Station 10-ALSEP area.–The penetration tests in this area were located close to the Rover at station 10 and along a line southwest to the ALSEP area (fig. 8-8). The ground surface in this region was generally level and free of large rock fragments.

Tests 1 and 2 (indexes 10 and 11, respectively) were performed with two different sized cones at adjacent locations. Figure 8-10(a) for the 3.22-cm^2 cone shows a soil of high penetration resistance to a depth of approximately 17.5 cm. The penetration resistance increases abruptly at this point, suggesting an even firmer layer, with a resistance to penetration greater than the recording capability of the SRP (215 N) but less than the ability of the astronaut to apply (250 N±), at least to a depth of 22 cm.

With the smaller cone (1.29 cm^2) used for test 2, it was possible to penetrate to a greater depth for a given applied force. The data (fig. 8-10(b)) show the same increase in resistance at a depth of 17.5 cm, below which the recording capacity of the penetrometer was exceeded.

Figure 8-10(c) for test 3 (index 12) again indicates a fairly firm soil overlying a harder layer, encountered here at a depth of 15 cm. The material appears to soften somewhat for the next 10 cm, but then becomes strong at 30 cm, as was true for test 2.

Test 4, index 13 (fig. 8-10(d)), located about midway between the Rover and the deep drill core, indicates a somewhat different stratigraphy, with a softer layer between depths of approximately 28 and 45 cm. The full recording capacity of the penetrometer had not been reached at the maximum penetration depth of 63 cm.

A preliminary stratigraphic profile (fig. 8-14) has been prepared with the cooperation of J. S. Nagle, based on (1) the X-radiographs of the drill-core stem and the station 10 core sample and (2) the penetration curves in figure 8-10. Five layers have been detected with varying thicknesses: surficial, hard, soft, harder, and rocky. This profile is qualitative in nature at this time and more quantitative analyses are planned.

Tests 6 and 7 (indexes 15 and 16, respectively) were plate-load tests (fig. 8-11). Because of the large plate-bearing area compared to the cone-base areas, penetration depths were less than those reached in the other tests. From the kinescopes, it is known that the surface soil at the site of test 7 is quite soft and that the lunar-reference plane penetrated to a depth of 1 or 2 cm. Average curves drawn through the data points in figure 8-11 are characteristic of a soil increasing in strength with depth.

Density and Porosity

Density and porosity values for the soil at different locations are available from analysis of several types of data. Conversion from density to porosity or vice versa requires a knowledge of the specific gravity of soil particles. Because this property has not yet been determined for the Apollo 16 samples, an average value of 3.05 has been assumed, based on the results of one test each on samples from

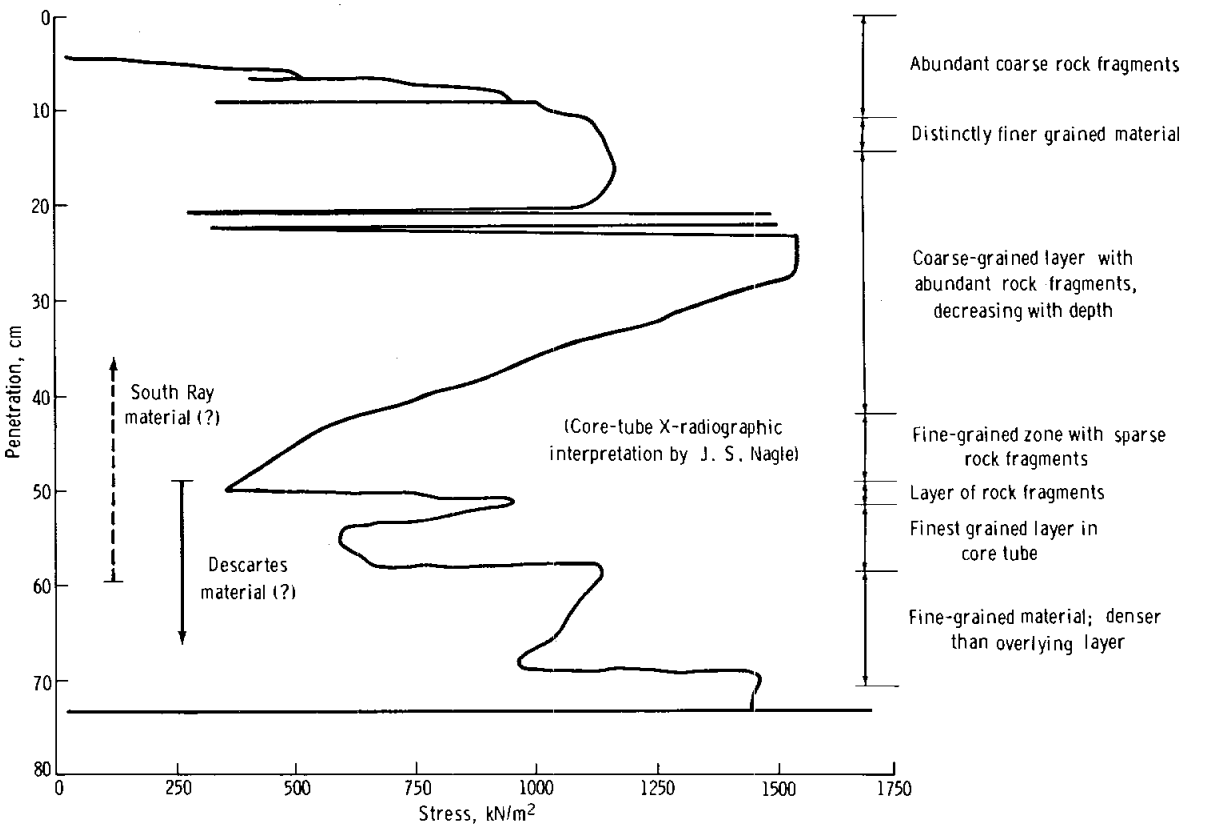

FIGURE 8-13.–Correlation of station 4 double-core-tube stratigraphy with SRP test 4 (index 8).

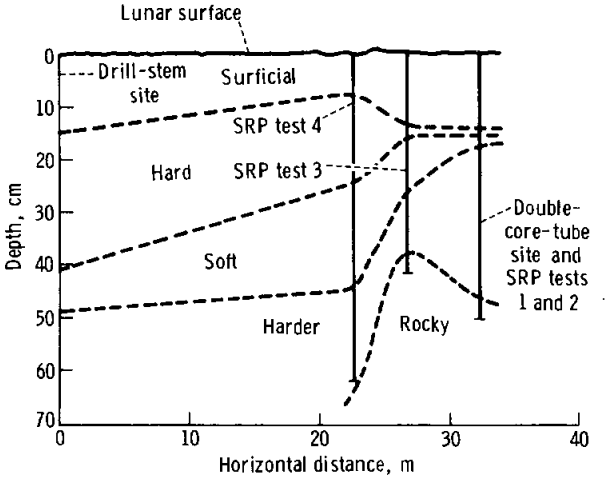

FIGURE 8-14.–Approximate soil profile between station 10 double-core-tube site and deep-drill-stem site in ALSEP area.

the Apollo 11, 12, and 15 missions, and tests on two Apollo 14 samples. Porosity n, density ρ, and specific gravity G_s are related according to

$$\rho = G_s(1 - n)\rho_w \qquad (8\text{-}4)$$

where ρ_w is the density of water.

Drive-tube samples.–Directly measured average densities for the drive-tube samples are presented in table 8-I. Although some correction may be required to give the in situ density because of sampling disturbance (refs. 8-7 and 8-8), these corrections should be small for tubes of the type used on Apollo 16. Density as a function of depth for these samples is shown in figure 8-15, assuming a constant density within each drive tube. Figure 8-16 shows smooth curves that have been fitted to the double-

core-tube density data according to

$$\rho = \rho_0 + k[\ln(z + 1)] \quad (8\text{-}5)$$

where ρ_0 is the density at the surface (g/cm^3), z is the depth (cm), and k is a densification factor. Such a relationship would be appropriate for densification under self-weight. The curves in figure 8-16 indicate that the surface soil can have a very low density (~0.9 g/cm^3) but the density will increase very rapidly with depth to a depth of 10 cm and then will increase more slowly thereafter. Below 20 cm, the density would generally be expected to be greater than 1.5 g/cm^3. However, these curves describe only a general trend; the actual distributions of density as a function of depth are certainly not monotonic and vary considerably in the lateral direction. This distribution is reflected in the character of the previously described tracings from the SRP.

The number of blows required to hammer the core tubes into the lunar surface generally increased with the density of the soil, as shown in table 8-I. The double core at station 10 required significantly more blows than the double core at station 10′, even though the density of both samples was nearly the same. This is attributable to the higher concentration of rock fragments in the soil at station 10, a difference observed also by the crewmen when they took rake samples at stations 10 and 10′.

Drill-stem samples.—Bulk densities for samples contained in the different sections of the drill stem are given in table 8-II. The initial density in the Apollo 16 drill stem has been reconstructed based on the hypothesis previously described, and the results and densities from the Apollo 15 drill stem are shown in figure 8-17. The Apollo 15 drill-stem-sample densities are significantly higher than those of the Apollo 16 drill stem. Furthermore, the character of the Apollo 15 density distribution is different from that of Apollo 16: the Apollo 15 density variation is erratic, whereas the Apollo 16 sample density generally increases with depth. It is likely that this difference is the result of different modes of deposition; perhaps the soil at the Apollo 16 drill-stem site was deposited in one large event, whereas the Apollo 15 stratigraphy was formed by multiple events.

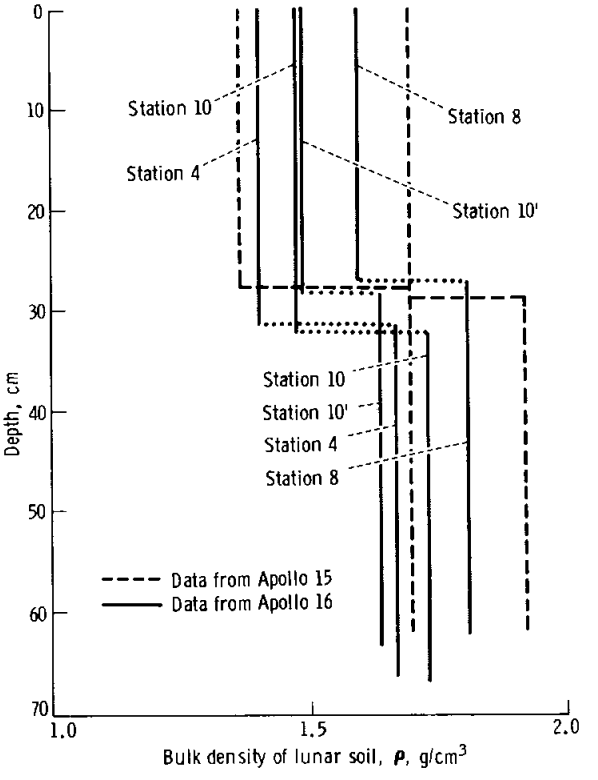

FIGURE 8-15.—Density as a function of depth relationships for drive-tube samples.

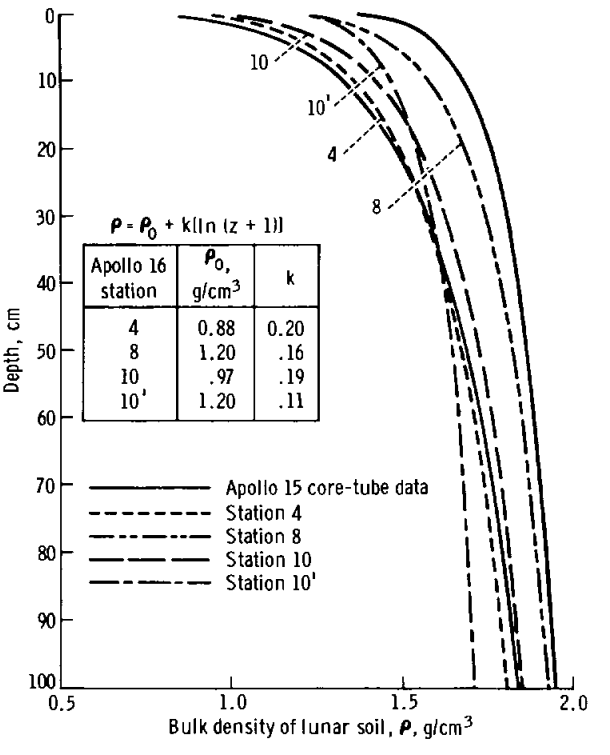

FIGURE 8-16.—Hypothetical relationships for density as a function of depth for homogeneous soil.

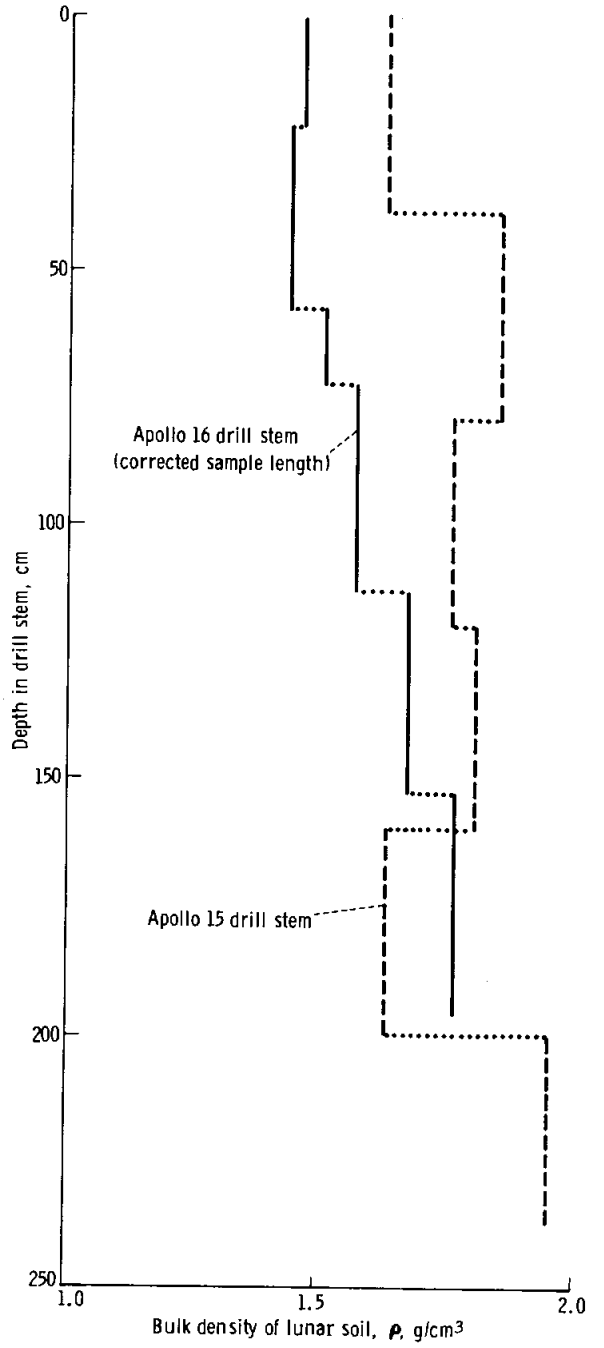

FIGURE 8-17.–Relationships of density as a function of depth for the Apollo 15 and Apollo 16 drill-stem samples.

Penetrometer results.–From simulation studies on soils having properties similar to those on the Moon, a correlation (ref. 8-5) has been developed between porosity and the average slope G_p (measured from the ground surface) of the curve representing cone-penetration resistance as a function of depth. This correlation was developed specifically for a 3.22-cm^2 (base area) cone; its application to results obtained when using cones of a different size or using a bearing plate has not yet been established. However, it has been assumed that, as a first approximation, the same correlation holds for the 1.29-cm^2 cone. A correlation has been developed for the 2.54 X 12.7 cm plate (ref. 8-12). Porosity and density estimates deduced in this way from the penetration curves in figures 8-9, 8-10, and 8-11 are given in table 8-IV.

The values of porosity derived in this way appear to be somewhat low, and the densities seem to be slightly high relative to the values for the core-tube samples. This variance in values could reflect a difference between the characteristics of the soil simulant and those of the actual lunar soil, which means that the correlation curve would be somewhat in error. Analyses on this point thus far are inconclusive. The results do show, however, that the densities at depths greater than a few centimeters are greater at station 10 than at station 4.

Footprint analysis.–Houston et al. (ref. 8-2) have used footprint depths to determine the porosity of the upper few centimeters of the lunar soil and have examined the variation in porosity at and among the Apollo landing sites on a statistical basis. A similar analysis has been applied to the Apollo 16 site. The correlation curve, based on the results of model tests and theoretical analyses (ref. 8-5), is shown in figure 8-18.

A total of 309 different footprints in the Apollo 16 photographs was studied, and the porosity variations were analyzed statistically, giving the results shown in table 8-V. A histogram of the porosity values is shown in figure 8-19. The values determined in this way reflect porosities only to depths of approximately 5 to 10 cm; that is, footprint depth is little affected by soil conditions below these depths.

From the results in table 8-V and figure 8-19 and from the results in reference 8-2, the following conclusions emerge.

(1) The variation of the average porosity of the soil near the surface is slight at the different locations.

TABLE 8-IV.–Porosity and Density Estimates Derived From Curves for Penetration Resistance as a Function of Depth

Station	*Test no.*	*Location*	*Penetrometer tip*	*Gradient of penetration-resistance curve, G_p, $kN/m^2/m$*	*Porosity, n, percent*	*Depth range, cm*	*Density, ρ, g/cm^3*
4	1	Uphill, south of Rover	3.22-cm^2 cone	3370 to 3860	37 to 39	0 to 20	1.86 to 1.92
4	2	On bench, south of Rover	1.29-cm^2 cone	1310 to 2280	41 to 43	0 to 25	1.74 to 1.80
4	3	On bench, southwest of Rover	1.29-cm^2 cone	2000 to 5200	36.5 to 41	0 to 25	1.80 to 1.94
4	4	Downhill, north of Rover	1.29-cm^2 cone	6700 to 10 000	32 to 35	0 to 20	1.98 to 2.07
10	1	Near Rover	3.22-cm^2 cone	[a]6300 to 9850	32 to 34	0 to 8	2.01 to 2.07
10	2	Near Rover	1.29-cm^2 cone	5600	35.5	0 to 25	1.96
10	3	Southwest of Rover on line to deep drill	1.29-cm^2 cone	4800 to 6850	34.5 to 36.5	0 to 25	1.93 to 2.00
10	6	Near Rover	2.54- by 12.7-cm plate		44 to 46	0 to 5	1.65 to 1.71
10	7	Near Rover	2.54- by 12.7-cm plate		42 to 44	0 to 5	1.71 to 1.77

[a]Penetrometer cone may have hit rocks.

TABLE 8-V.–Results of Statistical Analysis of Porosities Deduced From Footprint Depths

Location	*No. of observations*	*Mean porosity, percent*	*Standard deviation*
All data	309	45.1	3.0
All data except crater rims	273	45.0	2.8
Crater rims	36	46.1	4.6
ALSEP area[a]	59	45.2	3.9
LM area[a]	43	43.1	2.3
Station 1[a]	43	44.8	2.8
Station 4[a]	26	44.8	1.3
Stations 4 and 5[a]	35	45.8	2.6
Station 8[a]	20	45.0	2.3
Station 10[a]	15	45.2	2.1
Station 11[a]	12	43.7	1.5

[a]Crater rims excluded.

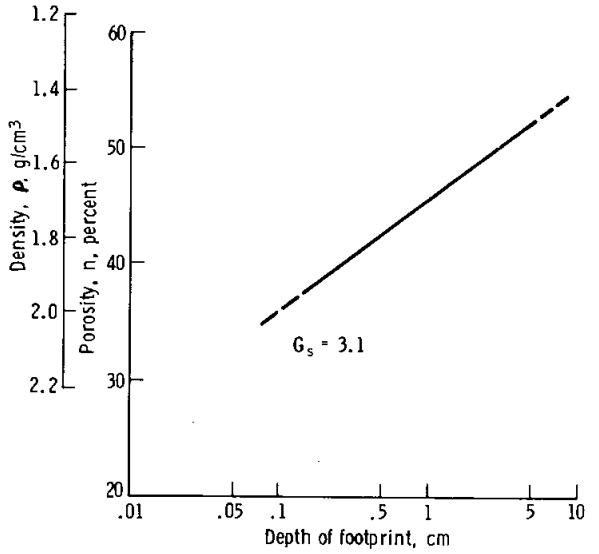

FIGURE 8-18.–Relationship between porosity of the upper few centimeters of lunar soil and footprint depth.

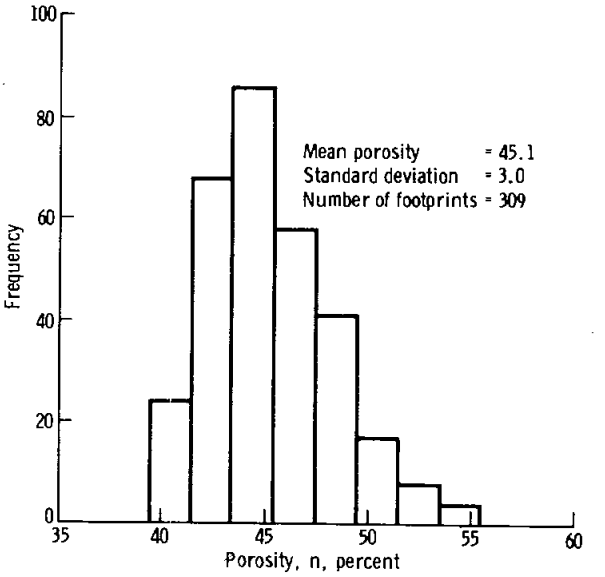

FIGURE 8-19.–Histogram of porosity variations at the Apollo 16 site as deduced from footprint depths.

(2) The average porosity (45.0 percent) of intercrater areas at the Apollo 16 site is slightly greater than that at the four previous Apollo sites (43.3 percent).

(3) The average porosity on crater rims at the Apollo 16 site (46.1 percent) is almost the same as that at the four earlier Apollo sites (46.7 percent).

(4) The standard deviation of porosities for the intercrater areas at the Apollo 16 site is the same as the average standard deviation (2.8 percent) for all previous lunar-landing missions.

(5) The standard deviation of porosities of crater rims is 4.6 percent at the Apollo 16 site as compared with the average of 4.0 percent for all previous sites. Thus, it is concluded that the lunar-soil surface has the same average porosity at all locations, regardless of composition or topography, although significant local (on a meter scale) variations may exist.

Density and porosity comparisons.–The density and porosity values deduced from the several data sources are compared in table 8-VI. From a study of these values, it appears that:

(1) Densities generally increase with depth.

(2) Densities deduced from footprints and penetrometer data are consistently higher and porosities are lower than those derived from core-tube-sample data. Studies of maximum and minimum densities based on simulation studies, tests on two 1-g samples of Apollo 14 soil and on one small sample of Apollo 15 soil, and studies of core-tube densities indicate that the correlations used to obtain densities and porosities from footprints and penetrometer data may give porosities that are too low by as much as 2 to 3 percentage points.

(3) Most probable values of soil porosity in the Descartes region of the Moon are in the range of 40 to 50 percent. Most values of density are likely to be between 1.5 and 1.8 g/cm^3.

Strength Characteristics

The penetration-resistance data in figures 8-9, 8-10, and 8-11 can be analyzed for evaluation of soil-strength characteristics (as indicated by cohesion c and angle of internal friction ϕ) by using the procedures described in the subsection entitled "Methods and Theory." Although the analyses completed to date represent only a preliminary study of the penetration curves, some results have been obtained and preliminary conclusions are possible for a comparison of strength-parameter relationships for the different tests.

Because the penetration-resistance curves indicate that the soil is not homogeneous with depth and because variations in lateral directions are sufficiently great to preclude direct comparison between the

TABLE 8-VI.–Summary of Lunar-Soil Density and Porosity Estimates

Location	Drive-tube samples			Drill-stem samples			Penetrometer data			Footprint analysis		
	Density, ρ, g/cm^3	Porosity, n, percent	Depth, z, cm (a)	Density, ρ, g/cm^3	Porosity, n, percent	Depth, z, cm (a)	Density, ρ, g/cm^3	Porosity, n, percent	Depth, z, cm (a)	Density, ρ, g/cm^3	Porosity, n, percent	Depth, z, cm (a)
LM area										1.73	43.1	0 to 10
Station 10	1.47	52	0 to 32				2.04	33	0 to 8	1.67	45.2	0 to 10
(between LM	1.72	43.5	32 to 65				1.97	35.5	0 to 25			
and ALSEP)							1.97	35.5	0 to 25			
							1.68	45	0 to 5			
							1.71	44	0 to 5			
Station 10'	1.48	51.5	0 to 28									
(between LM	1.63	46.5	29 to 63									
and ALSEP)												
ALSEP				1.46	52							
				1.43	53							
				1.56	49	0 to 223						
				1.66	45.5							
				1.75	42.5							
Station 1										1.69	44.8	0 to 10
Station 4	1.39	53.5	0 to 32				1.89	38	0 to 20	1.69	44.8	0 to 10
	1.66	45.5	32 to 66				1.77	42	0 to 25			
							1.87	39	0 to 25			
Station 8	1.59	48	0 to 27							1.68	45.0	0 to 10
Station 11										1.73	43.7	0 to 10

[a]Range for average porosities and densities indicated.

penetration-resistance curves for cones of two sizes (tests 1 and 2 at station 4 and tests 1 and 2 at station 10), a unique solution for c and ϕ is possible only in special cases. One such case is that of test 1 at station 4 (fig. 8-9(a)), which indicates relatively homogeneous soil with depth. For this case, application of equation (8-1) to the penetration resistance at two depths is possible, giving a simultaneous solution for c and ϕ. In most instances, however, results are presented in the form of plots of cohesion as a function of the friction angle required to give the measured penetration resistance for a given penetration depth. A soil-density value of 1.7 g/cm^3 has been assumed for the computations. The results are insensitive to the value assumed.

Station 4.—Strength parameters have been calculated for test 1 (index 5), performed uphill from the Rover, for the depth range of 10 to 20 cm, based on the assumption that the soil is homogeneous between these depths. The values obtained are 0.6 kN/m^2 and 46.5° for the c and ϕ, respectively. These values compare with c = 1.0 kN/m^2 and ϕ = 46° at a depth of 6 cm in the mare region (Hadley Plains) of the Apollo 15 site. Densities (based on cone-penetration-resistance gradient) at the two locations were almost the same: 1.97 g/cm^3 at the Apollo 15 location and 1.89 g/cm^3 at the location of test 1 at station 4. No evidence exists that grain-size distributions were significantly different at the two sites. Thus, the lower cohesion at the Apollo 16 station 4 location may reflect a different chemical and mineralogical composition for the soil at the site of test 1 on Stone Mountain than for the soil on the Hadley Plains.

Combinations of cohesion and friction angle that would account for measured values of penetration resistance for tests 2, 3, and 4 (indexes 6, 7, and 8,

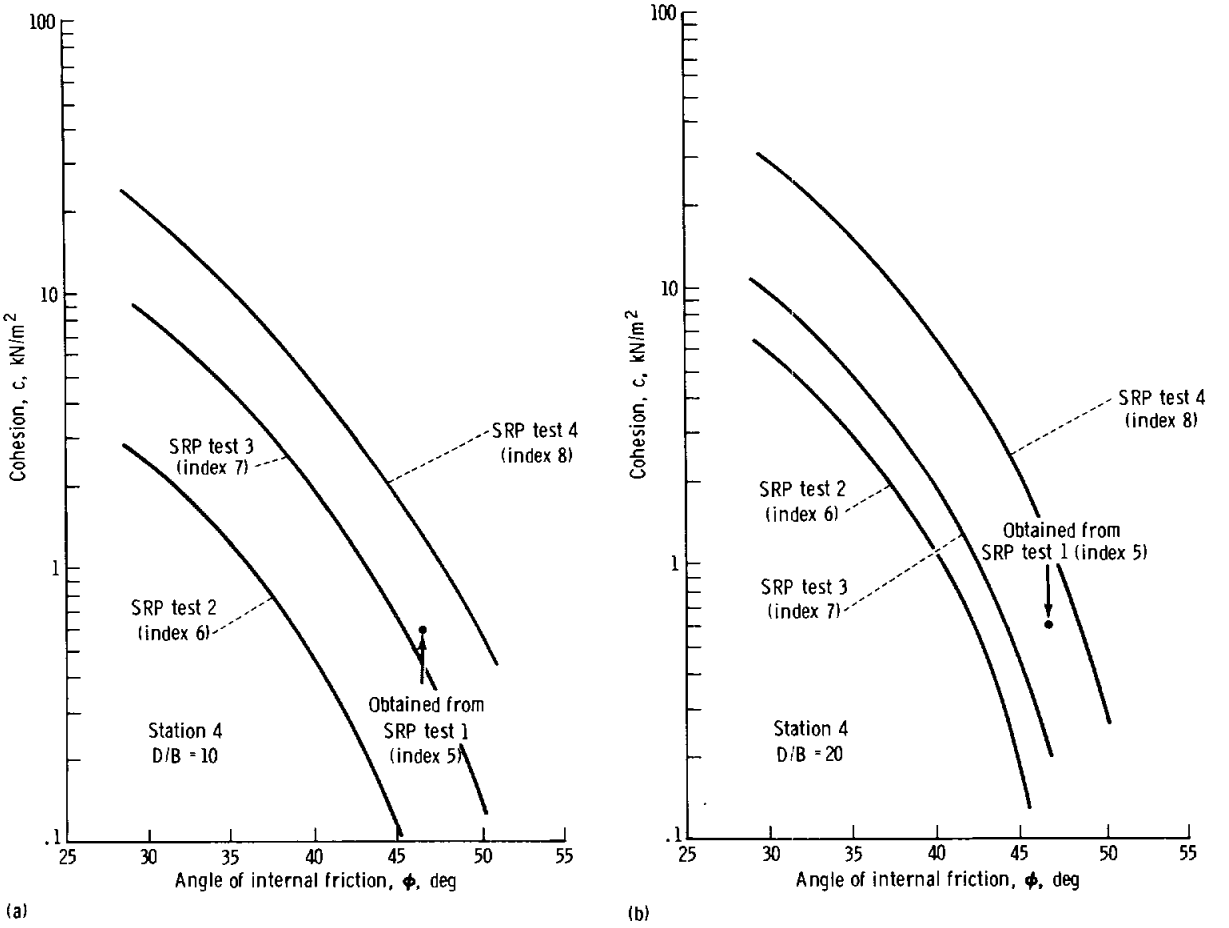

FIGURE 8-20.—Relationships of cohesion as a function of friction angle required to develop measured penetration resistances at station 4. (a) Depth of 12.8 cm. (b) Depth of 25.6 cm.

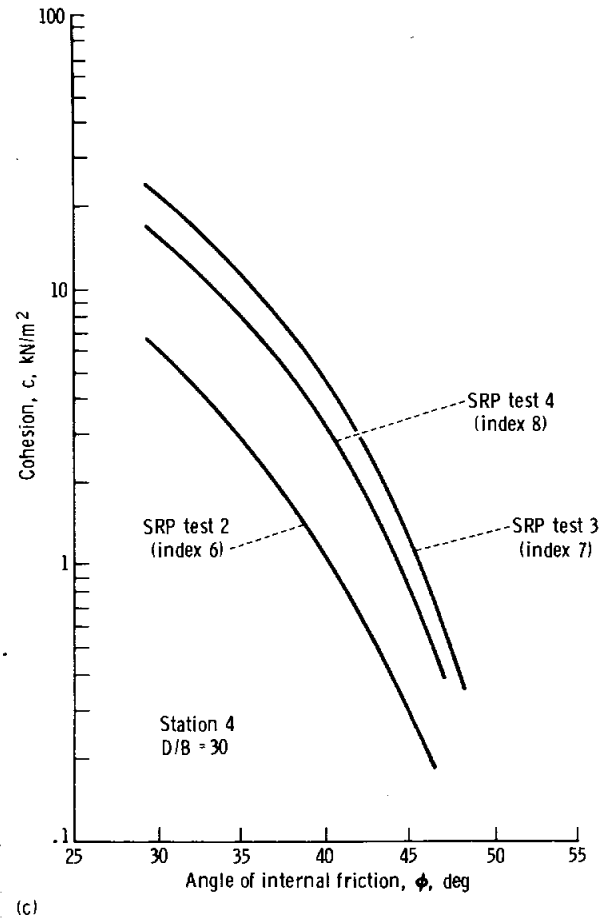

FIGURE 8-20.–Concluded. (c) Depth of 37.4 cm.

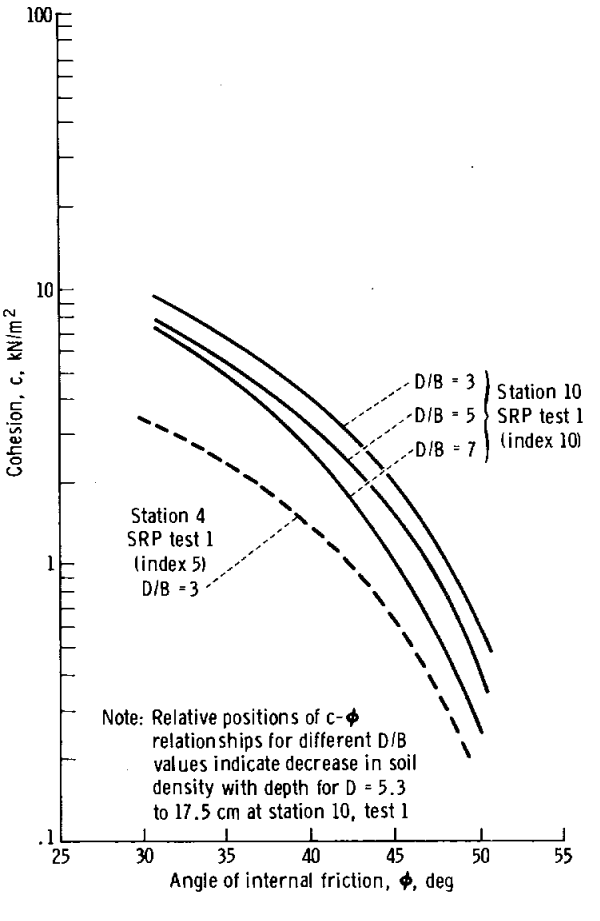

FIGURE 8-21.–Relationships of cohesion as a function of friction angle required to develop measured penetration resistances at station 10, test 1.

respectively) at station 4 are shown in figure 8-20. Relationships are shown for values of the ratio of depth to cone-base diameter (D/B) of 10, 20, and 30. These relationships are for actual depths of 12.8, 25.6, and 37.4 cm, respectively. A point is given on figures 8-20(a) and 8-20(b) to show the strength parameters for test 1 at depths of 10 and 20 cm.

A large difference exists in soil strength within the localized area of station 4. This variability is perhaps expected in view of the irregular sloping topography and relative abundance of large blocks on the surface (fig. 8-7(a)). However, low- and high-strength areas at depth are not readily discernible by observation of the surface or even on the basis of footprints. Thus, any generalizations concerning specific values of soil strength on sloping terrain would appear unwise, and each location should be investigated separately.

Station 10.–Shown in figure 8-21 are the c-ϕ relationships for the station 10 soil at the location of cone-penetration test 1 (index 10) for depths of 5.3 to 17.5 cm. These relationships indicate that soil strength (and probably density) decreases with depth. For a homogeneous soil deposit, a strength increase with depth would be expected.

Comparison between the strength characteristics for test 1 at station 4 and those of test 1 at station 10 (fig. 8-21), both determined by using the 3.22-cm^2 cone, shows that the soil at station 10 is considerably stronger at a depth of 6 cm.

Data from tests 2, 3, and 4 at station 10 (indexes 11, 12, and 13, respectively) indicate that strength varies only slightly between test locations for depths of 12.8 and 25.6 cm (fig. 8-22). Figure 8-10

shows, however, that the soil below a depth of 30 cm at the test 4 location does differ from that at the sites of tests 2 and 3.

The penetration-resistance data for tests 2 and 3 have been analyzed for specific values of c and ϕ (simultaneous solution of equation (8-2)), assuming homogeneous soil conditions between depths of 12.8 and 25.6 cm. Values obtained are given in table 8-VII, where values for test 1 at station 4 are also listed. These comparisons show comparable strengths and densities (based on the gradient of the curve for penetration resistance as a function of depth) for the three locations. An additional value of cohesion is given in table 8-VII, corresponding to that required to prevent collapse of the drill-stem hole at the ALSEP site, which stayed open to a depth of 2.18 m. The method of analysis (ref. 8-3) can be used to determine the cohesion needed to maintain an elastic state of stress in the soil around an open hole. For a Poisson ratio of 0.33, a soil density of 1.8 g/cm^3, and a friction angle of 46.5°, the calculated value of cohesion is 1.3 kN/m^2 at the bottom of a 2.18-m hole. This value of cohesion is at the upper limit of the values presented herein. However, the actual value of cohesion required to prevent collapse of the borehole could be much lower if plastic yielding of the hole occurs, as noted in reference 8-3.

The range in c-ϕ relationships for all tests at station 10 is compared with that at station 4 in figure 8-23. The much greater soil variability at station 4 is evident. Although strength variability appears to be less on plains than on slopes, no general conclusion is possible concerning whether the soil on slopes is weaker or stronger than that on the flat areas.

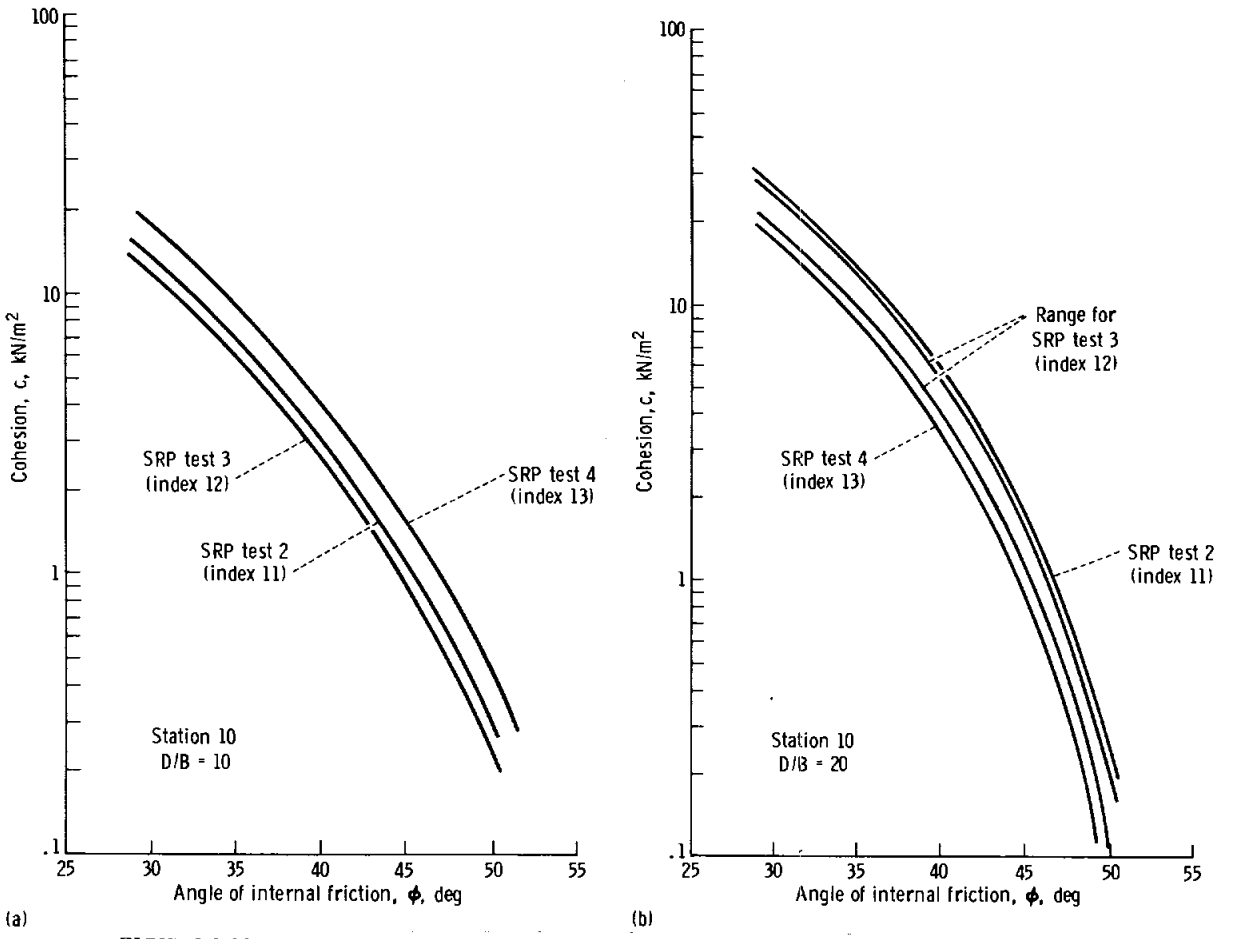

FIGURE 8-22.–Relationships of cohesion as a function of friction angle required to develop measured penetration resistances at station 10, tests 2, 3, and 4. (a) Depth of 12.8 cm. (b) Depth of 25.6 cm.

Preliminary analysis of the plate-load-test data, tests 6 and 7 at station 10 (fig. 8-11), indicates that strength and density are low at the surface but increase rapidly with depth.

TABLE 8-VII.–Strength Parameters at Three Locations

Station	Test no.	Index no.	Cohesion, c, kN/m^2	Friction angle, ϕ, deg	Density, ρ, g/cm^3
4	1	5	0.60	46.5	1.89
10	2	11	.37	49.5	1.96
10	3	12	.25 to .60	50 to 47	1.93
ALSEP	–	–	[a]1.3	[b]46.5	[c]1.75

[a]Based on open drill-hole analysis for a depth of 2.18 m.
[b]Assumed.
[c]Drill-stem sample.

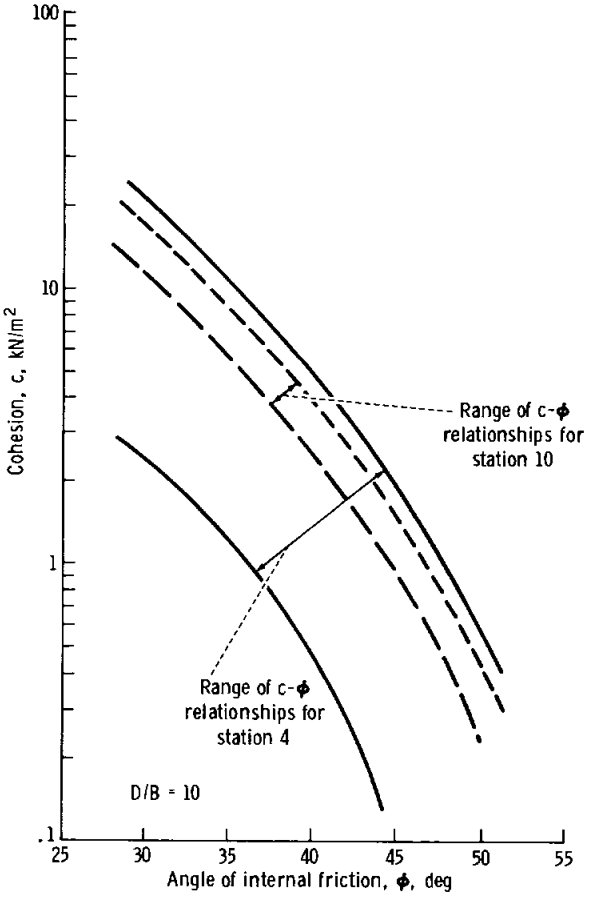

FIGURE 8-23.–Comparison of strength-parameter ranges, stations 4 and 10.

Soil Observations During LM Descent and Landing

During the final stages of descent, the LM crewmen reported the first signs of blowing dust between altitudes of 26 and 16 m above the lunar surface. However, the crewmen also indicated that the surface was clearly distinguishable all the way to touchdown and that no visibility difficulties were caused by the blowing dust. Examination of the descent movie confirms these comments. Indeed, blowing dust during the Apollo 16 landing seems to have caused the least visibility problem of all the Apollo LM landings to date.

As noted previously (ref. 8-3), the appearance of the moving dust sheet, caused by the interaction of the descent engine with the granular lunar surface, is a complex phenomenon. It depends on the small-scale nature of the surface, on the engine thrust, probably on the rate and angle of descent, on the viewer's location, and on the Sun angle. Not enough is yet known about the detailed structure of the lunar-surface material to determine if it varies significantly from site to site, so the effect of this factor cannot be assessed. Because the landing was delayed beyond the planned time, the Sun elevation was higher than on previous missions, and this may have contributed substantially to the improved viewing conditions.

Although detailed evaluation of the descent trajectory has not yet been completed, it is apparent that the vertical descent rate was somewhat higher than that of previous missions. From an altitude of 65 m to contact with the lunar surface, the elapsed time was less than 50 sec. The average descent velocity from an altitude of 65 to 26 m was approximately 1.7 m/sec; from 26 m to contact, the average velocity was approximately 1 m/sec. For the final 30 m of descent, this vertical velocity component was twice as great as that of the Apollo 15 landing, during which the last 18 m of descent were accomplished with a surface visibility of zero.

The actual landing was relatively soft with little or no stroking of the shock absorbers. Penetration of the footpads into the lunar surface was minimal, with the greatest penetration of 8 to 10 cm indicated for the −Y footpad on which the cosmic ray detector was mounted. The bottom panel of the detector was the only panel to which a small quantity of lunar dust adhered. The dust, presumably deposited on the panel during landing, is apparent to a height of

approximately 20 to 25 cm above the base of the pad or 10 to 15 cm above the lunar surface in the postlanding position of the footpad.

In contrast to the Apollo 15 landing, the descent-engine bell of the Apollo 16 LM did not appear to contact the lunar surface; the postlanding clearance was about 20 cm.

Slope Stability

Indications of downslope movement of surficial material can be seen in photographs of North Ray Crater as viewed from station 11. Figures 8-24 and 8-25 (photographs taken using the 60- and 500-mm lenses, respectively) show portions of the North Ray Crater wall. Maximum slope angles may be as great as 55° in rocky areas, although the slopes are probably not steeper than 40° to 45° in areas covered by what appears to be loose soil.

Distinct scarps and depressions where shallow slides have occurred in the upper crater walls are evident in figure 8-24. Other indications of downslope movement, shown in figures 8-24 and 8-25, include small gullies, a low crater density, and soil fillets on the uphill side of many rocks.

Preliminary studies of these features and other evidences of soil movement visible on other photographs, including fillets at the bases of large rocks, are in progress. The following preliminary observations have been made.

(1) If the slope angles are flatter than 45° where downslope movement of soil appears to be taking place, then the strength of the soil near the surface on these slopes must be less than that given by the parameters in table 8-VII.

(2) The steepest slopes in the north wall of North Ray Crater are rocky and may, in fact, be outcrops of a bench-forming rocky layer.

(3) The soil in fillets is probably fine grained and free of coarse particles.

(4) A sorting and segregation process appears to accompany the downslope movement of material. Talus slopes of both soil and coarser material have been identified (AS16-105-17228).

Further study of questions relating to slope stability, downslope movement of soil, and the properties of the soil on slopes is needed before definitive conclusions can be made.

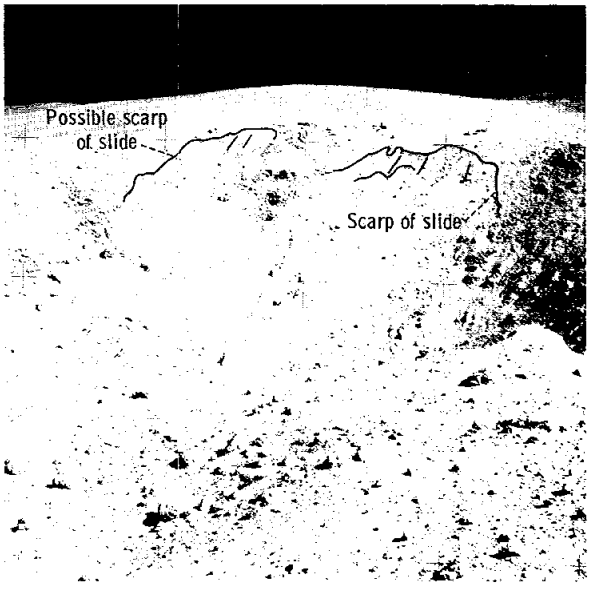

FIGURE 8-24.–View across North Ray Crater to the north showing slide areas near the top of the crater wall (AS16-106-17241).

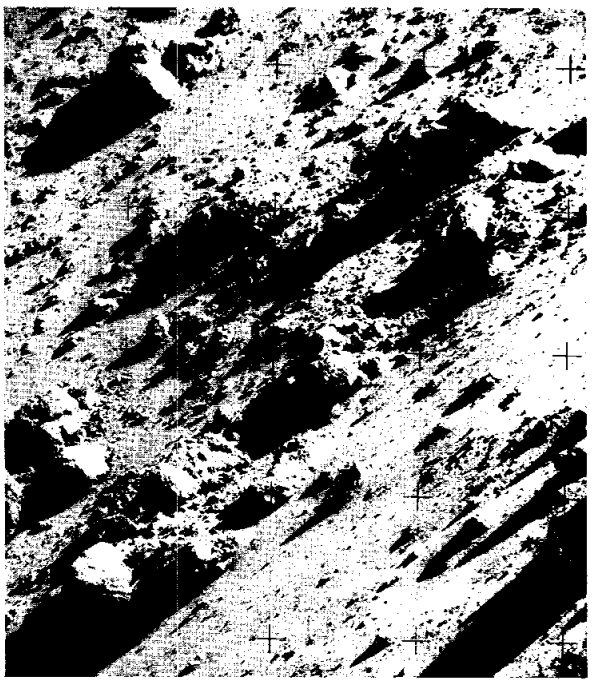

FIGURE 8-25.–A 500-mm photograph of the slope at North Ray Crater (AS16-105-17175).

Drillability of the Lunar Regolith

One probe hole for the heat-flow experiment was drilled to a depth of 2.34 ± 0.05 m in the ALSEP area. For premission drilling simulations, a crushed basalt was used as the drilling medium, leading to predicted rates shown in figure 8-26. The drilling time was 2.3 min, which is less by approximately a factor of 4 than the time obtained from figure 8-26, based on soil conditions at the Apollo 15 drilling site. The Apollo 16 drilling rate corresponded to that predicted for a typical mare plains site.

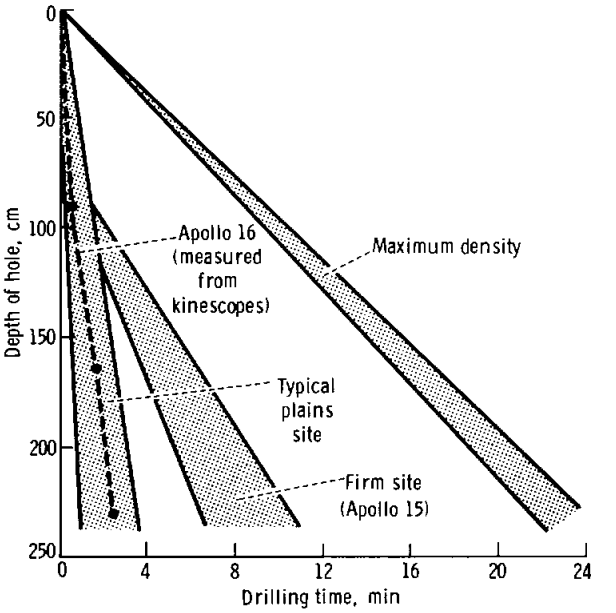

FIGURE 8-26.–Predicted compared to actual drilling time for heat-flow borestem.

Elastic Moduli and Seismic-Wave Velocities

From measurements on terrestrial sands and silts, it is known (ref. 8-13) that shear modulus G and effective confining pressure σ' are related according to

$$G = K(\sigma')^{1/2} \tag{8-6}$$

where K is a constant dependent on porosity. According to elastic theory, the shear-wave velocity v_s and the compression-wave velocity v_p are related to the shear modulus by

$$v_s = \sqrt{\frac{G}{\rho}} \tag{8-7}$$

$$v_p = \sqrt{\frac{\lambda + 2G}{\rho}} \tag{8-8}$$

where

ρ = density of the medium
λ = Lame constant = $2\upsilon G/(1 - 2\upsilon)$
υ = Poisson ratio

The profiles were obtained for the shear- and compression-wave velocities as a function of depth (fig. 8-27) with (1) the aid of the relationships between K, porosity, and shear strain given in reference 8-13; (2) an assumed shear strain of 10^{-4} percent for lunar seismic waves; (3) density profiles as shown in figure 8-16; (4) an at-rest lateral Earth pressure coefficient of 0.5; and (5) an assumed Poisson ratio of 0.28. The predicted low velocities in the upper few meters are consistent with the values measured in the active seismic experiment (ASE) at the Apollo 14 Fra Mauro landing site (ref. 8-14). These low velocities result from the low confining

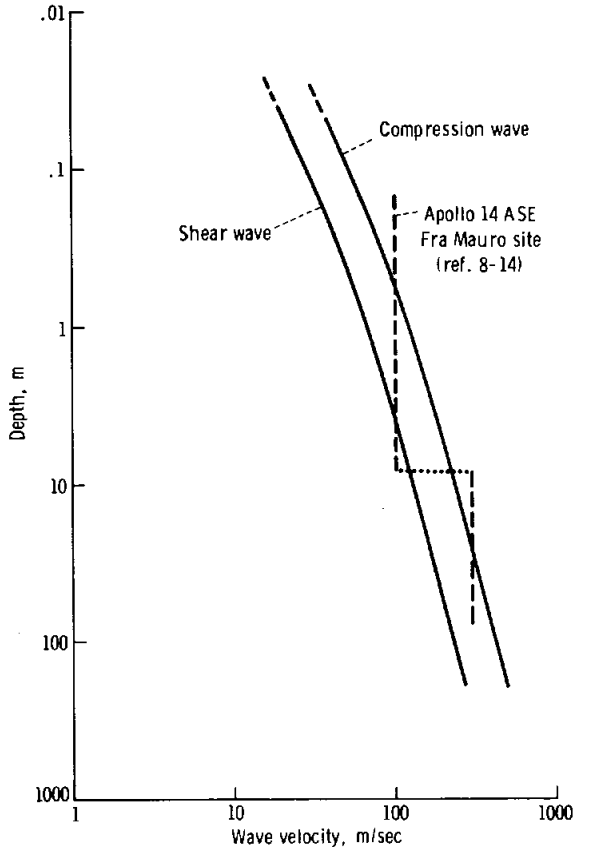

FIGURE 8-27.–Estimated seismic-wave velocities as a function of depth below the lunar surface.

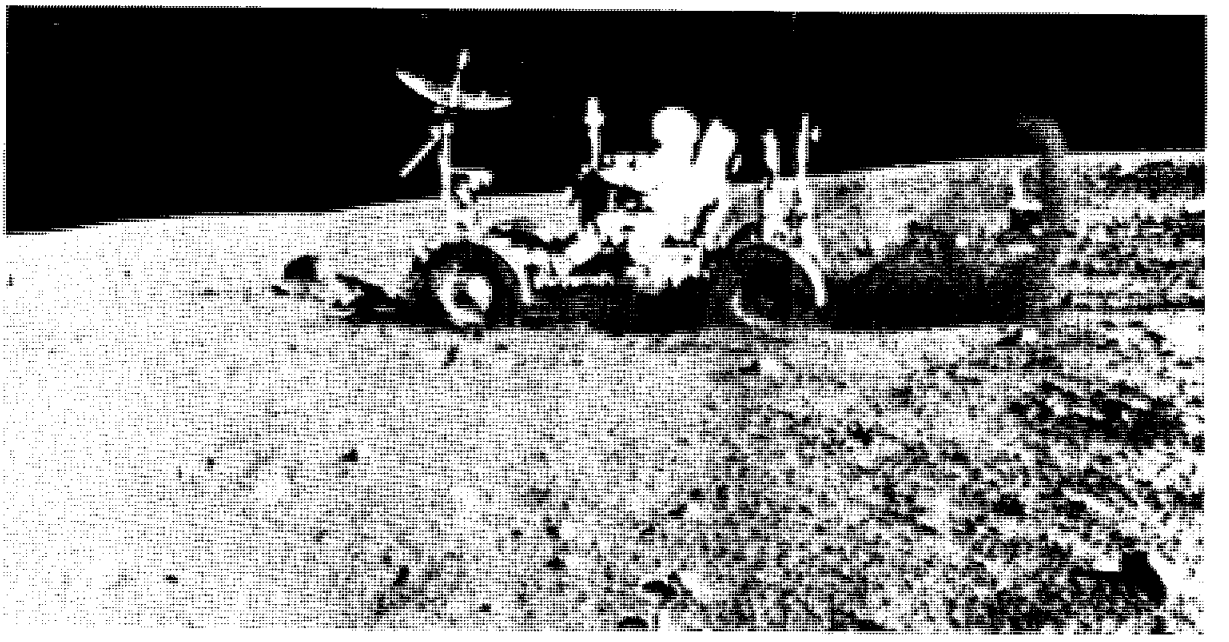

FIGURE 8-28.–Rover during Grand Prix. The "rooster tail" is indicative of a fine-grained, nearly cohesionless surficial soil (AS16-72-1718).

pressure σ' (which is a consequence of the low lunar-gravity field) rather than from unusual soil properties.

Soil and Rover Interaction

No direct quantitative information exists regarding the interaction of the Rover with the lunar surface while the vehicle was in motion. However, some information concerning the interaction of the vehicle with the lunar surface can be extracted from (1) crew descriptions; (2) photographic coverage of the extravehicular activities including 16-mm motion pictures taken with the data acquisition camera during the Grand Prix (fig. 8-28) and during parts of the Rover traverses while the vehicle was in motion; and (3) real-time read-outs from the Rover ampere-hour integrators and limited data from the navigation system components.

On the basis of crew observations and close examination of photographs of Rover tracks obtained throughout the mission, it appears that the vehicle developed excellent flotation and that the interaction between the wheels and the soil did not extend to any appreciable depth below the lunar surface. The observed wheel tracks ranged in depth from almost 0 to approximately 5 cm (at the rims of small fresh craters) with an average depth on the order of 1.25 cm. Further, the Rover wheels appear to have developed excellent traction with the lunar-surface material; in most cases, a sharp imprint of the chevron tread was clearly discernible, indicating that the surficial soil possessed some cohesion and that the amount of wheel slip was minimal.

The steepest slopes were encountered at Stone Mountain and near the edge of the rim of North Ray Crater. It appears that the Rover was operated on slopes ranging to 18°. Figure 8-3 shows such a slope at station 4. Extensive wheel-soil interaction tests performed with prototype Rover wheels on crushed-basalt lunar-soil simulants (refs. 8-15 and 8-16) indicate the maximum slope-climbing capability of the Rover to be within the slope-angle range of 19° to 23°. Further, the crew thought that, in negotiating the slope shown in figure 8-3, the Rover was approaching the limit of its slope-climbing capabilities.

In general, however, maneuvering the vehicle on slopes did not present any serious operational problems. The soil behavior appeared to reflect surficial deformation conditions and not any deep-seated soil movements. The vehicle could be

controlled more easily upslope than downslope. Some control problems were noted while driving downhill, especially at high speeds. (Maximum speed was 17 km/hr.)

Many photographs of Rover tracks were examined for variations in track depth, shape, and texture. Analysis of these tracks indicates that the regional variability in the consistency of the surficial soil throughout the Descartes site is less than that observed at the Hadley-Apennine region (Apollo 15). Accordingly, from a trafficability viewpoint, the surficial soil traversed by the Rover at the Descartes site may be considered relatively uniform on a regional scale. This uniformity does not preclude the significant local variations in soil consistency at depths greater than a few centimeters, as indicated previously from the results of core-tube, penetrometer, and deep drill tests.

Analyses of the average track depth (1.25 cm) by the methods developed by Freitag (ref. 8-17) yield an equivalent cone-penetration-resistance gradient G_p value of about 840 kN/m^2/m for the shallow depths influenced by the soil-wheel interaction. The values of the cone-penetration-resistance gradient presented in table 8-IV are somewhat greater than the derived equivalent value, but they represent soil characteristics to greater depths. Correcting for the gravity difference, the G_p value deduced from the Rover tracks corresponds to a crushed-basalt lunar-soil simulant on Earth having a porosity of approximately 41 percent. This porosity compares favorably with the porosity range (42 to 46 percent) calculated from the results of plate-load tests at station 10 (table 8-IV) and the statistical analysis of footprint depths (table 8-V).

CONCLUSIONS

The physical and mechanical properties of the soil at the Apollo 16 landing site are generally similar to those of the soils encountered at the previous Apollo sites. Data obtained using the self-recording penetrometer have provided a basis for quantitative study of stratigraphy, density, and strength characteristics. These results, in conjunction with crew observations, photography, and soil samples (particularly the core-tube samples), have been used to develop the following preliminary conclusions.

(1) Soil cover appeared to blanket all areas visited or observed at the Descartes landing area.

(2) Soil properties are variable on regional and local (1 m) scales.

(3) Visibility degradation by blowing dust was less during the Apollo 16 LM descent than during previous missions, probably due to a faster descent rate and a higher Sun angle rather than to different soil conditions.

(4) The grain-size distributions of soil samples from the Descartes area are comparable to those of samples from other areas of the Moon, although distributions for most Descartes samples fall toward the coarser edge of a composite distribution.

(5) The drive-tube samples indicate that soil density increases with depth, but the overall range of densities (1.40 to 1.80 g/cm^3) is slightly less than the range (1.36 to 1.91 g/cm^3) found for Apollo 15 core-tube samples.

(6) South Ray Crater material appears to cover the station 4 area to depths of 20 to 50 cm. Descartes Formation material may have been found at greater depths.

(7) Density distributions with depth for the Apollo 16 deep drill-stem samples are distinctly different from those of Apollo 15 and suggest that the modes of soil deposition at the two sites may have been different.

(8) Densities deduced from penetration-test data are slightly greater than but comparable to those obtained from core-tube samples.

(9) Statistical analysis of footprint depths indicates that for the soil near the surface (to depths of approximately 10 cm):

(a) Average porosity does not vary much for the different Apollo sites, although the average value is 45 percent at the Apollo 16 site as compared with 43.3 percent for each of the four previous Apollo sites.

(b) Average porosity on crater rims is somewhat greater (46.1 percent).

(10) At station 4 (Stone Mountain), the values for soil cohesion and friction angle are deduced to be 0.6 kN/m^2 and 46.5°, respectively.

(11) Variations in soil strength are great within short distances at station 4 on Stone Mountain. Because these variations appear to bear little relationship to local slope or surface appearance, generalizations concerning the strength of soils on sloping terrain are not possible.

(12) Less local variation in strength is evident at station 10 on the Cayley Plains than at station 4 on Stone Mountain.

(13) No general conclusion is possible concerning whether the soil on slopes is weaker or stronger than that on flat areas.

(14) Evidence exists for metastable slopes on the inner walls of North Ray Crater.

(15) The relatively low seismic-wave velocities for the upper few meters of the lunar surface measured in the active seismic experiment can be accounted for in terms of the low confining pressure resulting from the low lunar-gravity field.

(16) The Rover performed quite satisfactorily in all maneuvers attempted at the Descartes site. Lunar-soil parameters deduced from observed wheel-soil interactions agree well with those obtained by other methods for shallow depths.

It is expected that information on soil properties obtained thus far will be useful in the future for several types of soil-property-dependent lunar studies.

SUMMARY

The purpose of the soil mechanics experiment is to determine the physical characteristics of the lunar soil to depths of several decimeters and their variations in lateral directions, on slopes, and between different regions of the Moon. Soil mechanics data were derived from television, surface photography, core-tube samples, and measurements using the SRP. Simulation studies and soil mechanics theories have been used to deduce information concerning soil density and strength characteristics and their variations from place to place.

Soil properties are variable on regional and local (1 m) scales in the Descartes area although, in general, the soil grain-size distributions and densities are comparable to those of samples from other areas of the Moon. The overall density range was from about 1.4 to 1.8 g/cm^3. The average porosity of the upper 10 cm of soil at the Descartes site is estimated at 45 percent as compared with 43.3 percent for each of the four previous Apollo sites.

At one location on Stone Mountain, the values for soil cohesion and friction angle are deduced to be 0.6 kN/m^2 and 46.5°, respectively, although variations in strength are great within short distances at this location. These variations bear little relationship to local slope or surface appearance; thus, generalizations concerning the strength of soils on sloping terrain are not possible. No general conclusion is possible concerning whether the soil on slopes is weaker or stronger than that on flat areas, although the soil strength in level areas seems less variable. Some evidence exists for soil instability on the inner walls of North Ray Crater. Based on the known behavior of terrestrial soils of comparable gradation and density to that on the Moon, seismic P-wave velocities on the order of 100 m/sec are to be expected for the upper few meters of the lunar surface, increasing to about 300 m/sec at depths of 50 to 80 meters.

APPENDIX

BEARING CAPACITY FACTORS FOR CONE-PENETRATION RESISTANCE

From the results of model tests (ref. 8-10), it has been found that a failure surface as shown in figure 8-2 represents closely the actual failure surface associated with wedge penetration.

The angle γ, which defines the plane shear zone OAC, depends on the penetrometer-to-soil friction angle δ and soil friction angle ϕ and can be determined from

$$\tan\delta[1 + \sin\phi \sin(2\gamma - \phi)] - \sin\phi\cos(2\gamma - \phi) = 0 \qquad \text{(A-1)}$$

Values of γ determined from equation (A-1) for different values of ϕ and δ/ϕ are presented in reference 8-10. A logarithmic spiral bounds a radial shear zone to a point of vertical tangency at point E, above which the failure surface rises vertically to the ground surface. For large depths of penetration, such as shown in figure 8-2, the angle β, which locates point E, equals ϕ. For shallow penetration depths, the logarithmic spiral breaks out at ground surface before vertical tangency is reached, and the corresponding value of β can be determined iteratively.

Equilibrium analysis of the failure zone shown in figure 8-2 leads to

$$q_f = cN_c\xi_c + B\gamma_s N_{\gamma q}\xi_{\gamma q} \qquad \text{(A-2)}$$

where

q_f = ultimate unit tip resistance
c = unit cohesion
B = penetrometer base width or diameter
γ_s = unit weight of soil
N_c, $N_{\gamma q}$ = bearing capacity factors
ξ_c, $\xi_{\gamma q}$ = shape factors

For wedges, the bearing capacity factors N_c and $N_{\gamma q}$ are given in reference 8-10 as

$$N_c = f_1\left(\frac{D}{B}, \phi, \alpha, \frac{\delta}{\phi}\right) = \frac{1 + \sin\phi \sin(2\gamma - \phi)}{\sin\phi \cos\phi} \exp\left(2\theta_0 \tan\phi\right) - \frac{1}{\tan\phi} + \frac{\cos(2\gamma - \phi)\tan\psi}{\cos\phi} \exp\left(2\theta_0 \tan\phi\right) \qquad \text{(A-3)}$$

$$N_{\gamma q} = f_2\left(\frac{D}{B}, \phi, \alpha, \frac{\delta}{\phi}\right) = \frac{\cos(\psi - \delta)}{\cos\delta} \frac{[1 + \sin\phi \sin(2\gamma - \phi)]}{\cos\phi \cos(\gamma - \phi)} \left[\frac{1}{4} \frac{\cos^2(\gamma - \phi)}{\cos^2\psi \cos^2\phi} \times I_\theta + \frac{3}{4} \frac{\cos(\gamma - \phi)}{\cos\psi \cos\phi} \times \cos^2\beta \exp\left(2\theta_0 \tan\phi\right) \left(m - \frac{2}{3} m'\right) - (1 - \sin\phi) \frac{\cos\psi \cos\phi}{\cos(\gamma - \phi)} (m - m')^2 (m + 2m') + K \frac{\cos\psi \cos\phi}{\cos(\gamma - \phi)} m^3\right] - \frac{\tan\psi}{4} \qquad \text{(A-4)}$$

where

D = depth of penetrometer base below ground surface
ϕ = soil friction angle
$\psi = 90° - \alpha$
α = half the wedge apex angle
δ = soil-to-penetrometer friction angle
γ = the topmost angle of the plane shear zone
$\theta_0 = 180° - (\gamma + \psi) + \beta$
K = lateral Earth-pressure coefficient
m = D/B (relative depth)
$m' = D_\beta/B = 1/2 \sin\beta \cos(\gamma - \phi)/\cos\psi \cos\phi \exp(\theta_0 \tan\phi)$

D_β = vertical position of point E on the failure surface above base level (see fig. 8-2)

and $I_\theta = \frac{1}{1 + 9\tan^2\phi} \{3 \tan\phi [\exp(3\theta_0 \tan\phi) \cos\beta - \cos(\theta_0 - \beta)] + [\exp(3\theta_0 \tan\phi) \sin\beta + \sin(\theta_0 - \beta)]\}$ (A-5)

The bearing capacity factors for cones can be determined by using the bearing capacity factors for wedges modified by the shape factors computed according to equations (8-2) and (8-3).

REFERENCES

8-1. Mitchell, J. K.; Scott, R. F.; Houston, W. N.; Costes, N. C.; et al.: Mechanical Properties of Lunar Soil: Density, Porosity, Cohesion, and Angle of Internal Friction. Proceedings of the Third Lunar Science Conference, vol. 3, David R. Criswell, ed., MIT Press (Cambridge, Mass.), 1972.

8-2. Houston, W. N.; Hovland, H. J.; Mitchell, J. K.; and Namiq, L. I.: Lunar Soil Porosity and Its Variation as Estimated From Footprints and Boulder Tracks. Proceedings of the Third Lunar Science Conference, vol. 3, David R. Criswell, ed., MIT Press (Cambridge, Mass.), 1972.

8-3. Mitchell, J. K.; Bromwell, L. G.; Carrier, W. D., III; Costes, N. C.; et al.: Soil-Mechanics Experiment. Sec. 7 of Apollo 15 Preliminary Science Report. NASA SP-289, 1972.

8-4. Leonovich, A. K.; Gromov, V. V.; Rybakov, A. V.; Petrov, V. K.; et al.: Studies of Lunar Ground Mechanical Properties With the Self-Propelled "Lunokhod-1." Ch. 8 of Peredvizhnaya Laboratoriya na Luna-Lunokhod-1. (Translation by Joint Publ. Res. Service, JPRS 54525, 1971, pp. 120-135.)

8-5. Houston, W. N.; and Namiq, L. I.: Penetration Resistance of Lunar Soils. J. Terramechanics, vol. 8, no. 1, 1971, pp. 59-69.

8-6. Costes, N. C.; Cohron, G. T.; and Moss, D. C.: Cone Penetration Resistance Test – An Approach to Evaluating the In-Place Strength and Packing Characteristics of Lunar Soils. Proceedings of the Second Lunar Science Conference, vol. 3, A. A. Levinson, ed., MIT Press (Cambridge, Mass.), 1971, pp. 1973-1987.

8-7. Houston, W. N.; and Mitchell, J. K.: Lunar Core Tube Sampling. Proceedings of the Second Lunar Science Conference, vol. 3, A. A. Levinson, ed., MIT Press (Cambridge, Mass.), 1971, pp. 1953-1958.

8-8. Carrier, W. D., III; Johnson, S. W.; Werner, R. A.; and Schmidt, R.: Disturbance in Samples Recovered with the Apollo Core Tubes. Proceedings of the Second Lunar Science Conference, vol. 3, A. A. Levinson, ed., MIT Press (Cambridge, Mass.), 1971, pp. 1959-1972.

8-9. Scott, R. F.: Principles of Soil Mechanics. Addison-Wesley (Reading, Mass.), 1963.

8-10. Durgunoglu, H. T.: Static Penetration Resistance of Soils. Ph. D. Dissertation, Univ. of Calif. at Berkeley, 1972.

8-11. Gast, P. W.; Haskin, L. A.; and Wasserburg, G. J.: Introduction. Earth Planet. Sci. Letters, vol. 13, no. 2, Jan. 1972, pp. 223-224.

8-12. Namiq, L. I.: Stress-Deformation Study of a Simulated Lunar Soil. Ph. D. Dissertation, Univ. of Calif. at Berkeley, 1970.

8-13. Seed, H. B.; and Idriss, I. M.: Soil Moduli and Damping Factors for Dynamic Response Analyses. Rept. EERC 70-10, Earthquake Engineering Res. Center, Univ. of Calif. at Berkeley, 1970.

8-14. Kovach, Robert L.; Watkins, Joel S.; and Landers, Tom: Active Seismic Experiment. Sec. 7 of Apollo 14 Preliminary Science Report. NASA SP-272, 1971, pp. 163-174.

8-15. Green, A. J.; and Melzer, K. J.: Performance of the Boeing LRV Wheels in a Lunar Soil Simulant: Effect of Wheel Design and Soil. Tech. Rept. M-71-10, Rept. 1, USAE WES, Vicksburg, Miss., 1971.

8-16. Melzer, K. J.: Performance of the Boeing LRV Wheels in a Lunar Soil Simulant: Effect of Speed, Wheel Load, and Soil. Tech. Rept. M-71-10, Rept. 2, USAE WES, Vicksburg, Miss., 1971.

8-17. Freitag, Dean R.: A Dimensional Analysis of the Performance of Pneumatic Tires on Soft Soils. Tech. Rept. 3-688, USAE WES, Vicksburg, Miss., 1965.